

# **DYNAMIC COMPLEXATION-CAPILLARY ELECTROPHORESIS**

**DYNAMIC COMPLEXATION-CAPILLARY  
ELECTROPHORESIS: AN INTEGRATIVE  
BIOPHYSICAL TOOL FOR THERMODYNAMIC  
ANALYSIS OF BIOMOLECULAR INTERACTIONS**

By

GISELLE SEGUÍ-LINES, B.S.

A Thesis

Submitted to the School of Graduate Studies

In Partial Fulfillment of the Requirements

for the Degree

Master of Science

McMaster University

© Copyright by Giselle Seguí-Lines, December 2009

MASTER OF SCIENCE (2009)

McMaster University  
Chemistry and Chemical Biology  
Hamilton, Ontario

TITLE: Dynamic Complexation-Capillary Electrophoresis: An Integrative  
Biophysical Tool For Thermodynamic Analysis Of Biomolecular  
Interactions

AUTHOR: Giselle Seguí-Lines

SUPERVISOR: Professor Dr. Philip Britz-McKibbin

NUMBER OF PAGES: xiii, 113

## **ABSTRACT**

Capillary electrophoresis is a high resolution microseparation technique that is increasingly being recognized as a physical tool to characterize biomolecular interactions, where dynamic complexation of analytes with discrete additives is used to resolve complex mixtures of solutes, including enantiomers. Despite the wide interest in developing high-throughput screening platforms for drug discovery or disease prognosis, little emphasis has been placed on enhancing “pre-analysis steps” that are often the most crucial component determining the overall performance of a method. Off-line sample pretreatment protocols for complex biological samples are often time-consuming and not amenable for automation. The major goal of this thesis is the development of a single-step analytical platform by CE for targeted metabolites that integrate several different sample pretreatment processes during separation, which can also be used to characterize the thermodynamic parameters associated with covalent and non-covalent interactions. Two distinct projects in this thesis have been examined involving boronic acid-polyol and protein-cyclic nucleotide interactions that illustrate the concept of integrating sample pretreatment with chemical analysis based on dynamic complexation-capillary electrophoresis.



The first project consists of a new strategy for enhancing target selectivity when using 3-nitrophenylboronic acid as an electrokinetic probe in dynamic complexation-capillary electrophoresis. The differential migration of ternary boronate ester complexes permits the selective analysis of micromolar levels of UV-transparent polyol stereoisomers in urine samples that is applicable to single-step screening of in-born errors of sugar metabolism, such as galactosemia. In the second project, the impact of ligand binding on protein stability is assessed by dynamic ligand exchange-affinity capillary electrophoresis with laser-induced native fluorescence detection. This is a convenient yet rapid format for comparative thermodynamic studies of a regulatory subunit of protein kinase involving different cyclic nucleotide analogues without off-line sample pretreatment, since ligand exchange and protein unfolding processes are integrated in-capillary during electromigration.

## **ACKNOWLEDGEMENTS**

I am so thankful to my professor Dr. Philip Britz-McKibbin for the trust and encouragement to pursue this dream that has become true. I would also like to thank Dr. Saravanamuttu, Dr. Hileman and Dr. Brennan for each and every committee meeting, where I had the opportunity to present my work and receive your questions and advices in an environment of respect and scientific stimuli. All my gratitude to Dr. Murray Potter for his contributions on the organization and proof-reading of the thesis draft. Thanks to my co-workers Jennilee Gavina, Adam Ptolemy, Jason D'Amaral and Claire Kaise for the team atmosphere in which I have had the pleasure to work.

Thanks to my husband Sergio for his continuous support, for all the sacrifices and the daily encouragement that I could do this. To my kids Alex, Stefan and Sofia, to whom this work is especially dedicated: you always remember to give the most of you, and to push all the limits to reach your goals and your dreams. To my sister Ginete, for being in my life again, helping me in the difficult moments. To all my friends, the ones that I can see everyday and the ones that are at all times there for me, at an e-mail or a phone call distance, for backing me up and reassuring me when I doubted myself. And last, but not least, to my parents, because they

always taught me with so much love that the only path is the one we are able to build ourselves with perseverance, wisdom and dedication.

## TABLE OF CONTENTS

<b>DYNAMIC COMPLEXATION-CAPILLARY ELECTROPHORESIS: AN INTEGRATIVE BIOPHYSICAL TOOL FOR THERMODYNAMIC ANALYSIS OF BIOMOLECULAR INTERACTIONS .....</b>	<b>I</b>
<b>ABSTRACT.....</b>	<b>III</b>
<b>ACKNOWLEDGEMENTS .....</b>	<b>V</b>
<b>TABLE OF CONTENTS.....</b>	<b>VII</b>
<b>TABLE OF FIGURES.....</b>	<b>IX</b>
<b>LIST OF TABLES .....</b>	<b>X</b>
<b>LIST OF ABBREVIATIONS .....</b>	<b>XI</b>
<b>CHAPTER I .....</b>	<b>1</b>
<b>1.BACKGROUND .....</b>	<b>1</b>
1.1 INTRODUCTION.....	2
1.2 CE: A VERSATILE TECHNIQUE? .....	3
1.3 ELECTROPHORESIS IN A CAPILLARY? .....	5
1.4 INSTRUMENTATION IN CE ANALYSIS.....	6
1.5 ELECTROPHORETIC MOBILITY AND ELECTROSMOTIC FLOW.....	7
1.6 ELECTROPHORETIC MOBILITY .....	9
1.7 ELECTROSMOTIC FLOW (EOF) .....	10
1.8 APPARENT MOBILITY .....	14
1.9 SEPARATION EFFICIENCY AND RESOLUTION .....	17
1.10 DYNAMIC COMPLEXATION USING ADDITIVES IN CE.....	19
1.10.1 Theory .....	20
1.11 RESEARCH OBJECTIVES.....	25
<b>CHAPTER II .....</b>	<b>28</b>
<b>2. ELECTROKINETIC PROBES FOR SINGLE-STEP SCREENING OF POLYOL STEREOISOMERS: THE VIRTUES OF TERNARY BORONATE ESTER COMPLEX FORMATION.....</b>	<b>28</b>
2.1 ABSTRACT .....	29
2.2 INTRODUCTION.....	29
2.3 RESULTS AND DISCUSSION.....	30
2.4 CONCLUSIONS .....	39
2.5 REFERENCES .....	40
<i>ELECTRONIC SUPPLEMENTAL INFORMATION.....</i>	<i>41</i>
2.6 EXPERIMENTAL .....	41

2.6.1 Chemicals and Reagents.....	41
2.6.2 Apparatus and Conditions .....	42
2.6.3 Central Composite Experimental Design .....	43
2.6.4 NMR Spectroscopy .....	43
2.6.5 Human Urine Analysis .....	44
2.7 THEORY.....	45
2.7.1 $pK_a$ Determination by DC-CE.....	45
2.8 CENTRAL COMPOSITE DESIGN FOR SEPARATION OPTIMIZATION.....	48
2.9 ROLE OF PHOSPHATE AND NPBA IN THE DIRECT UV DETECTION OF POLYOLS.....	53
2.10 NMR STUDIES OF TERNARY COMPLEX FORMATION. ....	55
2.11 METHOD VALIDATION .....	57
<b>CHAPTER III .....</b>	<b>60</b>
<b>3. HIGH-THROUGHPUT SCREENING OF HOLOPROTEIN CONFORMATIONAL STABILITY BY DYNAMIC LIGAND EXCHANGE- AFFINITY CAPILLARY ELECTROPHORESIS .....</b>	<b>60</b>
3.1 ABSTRACT .....	61
3.2 INTRODUCTION .....	61
3.3 THEORY .....	63
3.4 RESULTS AND DISCUSSION.....	66
3.5 CONCLUSIONS .....	70
3.6 REFERENCES .....	71
3.7 FOOTNOTES .....	72
<b>CHAPTER IV.....</b>	<b>77</b>
<b>4. FUTURE APPLICATIONS AND DIRECTIONS.....</b>	<b>78</b>
<b>CHAPTER V.....</b>	<b>86</b>
<b>5. APPENDIX .....</b>	<b>86</b>
5.1 COVALENT BORONATE ESTER COMPLEXATION.....	87
5.1.1 Introduction .....	87
5.1.2 $pK_a$ and binding constant determination .....	88
5.1.3 Effect of substituents on $pK_a$ of boronic acids .....	89
5.1.4 Sensors for Saccharides .....	92
5.1.5 Polyols: Significance and Metabolism .....	96
5.2 PROTEIN UNFOLDING AND CNT INTERACTIONS .....	98
5.2.1 cAMP-dependent Protein Kinase: Structure and biological role. ....	98
5.2.2 Principles of Protein Unfolding.....	100
5.2.3 Classical models of protein unfolding .....	103
5.2.4 Urea Protein Unfolding Dynamics .....	105
5.2.5 Protein Unfolding Time Regime.....	107

## TABLE OF FIGURES

<b>Figure 1.1</b> Schematic diagram of a CE instrument.....	7
<b>Figure 1.2</b> Debye-Hueckel-Stern model of the electric double layer .....	12
<b>Figure 1.3</b> Flow profile in CE and in HPLC.....	14
<b>Figure 1.4</b> Ion migration order in CE. ....	15
<b>Figure 2.1</b> Dynamic complexation model depicting NPBA as an electrokinetic probe for polyols in phosphate buffer by DC-CE.....	31
<b>Figure 2.2</b> Electropherograms of the increase in $\mu_{ep}^A$ of the NPBA-sorbitol complex relative to free NPBA .....	32
<b>Figure 2.3</b> Electropherogram overlay of the impact of increasing [NPBA] in phosphate for single-step analysis of polyols by DC-CE.....	35
<b>Figure 2.4</b> Electropherogram of single-step screening of urinary polyols.....	38
<b>Figure 2.5</b> Electropherograms of the impact of increasing NPBA concentration in the BGE for the separation and detection of polyols by DC-CE.....	46
<b>Figure 2.6</b> CCD for optimization of resolution response of hexitols.....	50
<b>Figure 2.7</b> Surface response models for the optimization of polyol resolution ...	51
<b>Figure 2.8</b> Electropherograms of the impact of phosphate concentration of the absorbance response of polyols.....	54
<b>Figure 2.9</b> (a) $^{31}\text{P}$ -NMR and (b) $^{11}\text{B}$ -NMR spectra of chemical shift changes for phosphate at pH 6.8 as a function of electrolyte composition. ....	57
<b>Figure 3.1</b> Three-step process of dynamic cAMP-stripping, cNT exchange and <i>holo</i> -RI $\alpha$ -cNT unfolding by DLE-ACE. ....	64
<b>Figure 3.2</b> Impact of ligand on conformational stability of RI $\alpha$ .....	67
<b>Figure 4.1</b> Resolution of C4, C5 and C7-polyols using two different [NPBA] .....	80
<b>Figure 4.2</b> Impact of cNT binding on the conformational stability of EPAC upon urea denaturation by DLE-ACE.....	83
<b>Figure 5.1</b> The relationships between boronic acid and its diol ester.....	89
<b>Figure 5.2</b> Chemical structures of neutral stereoisomers of hexitols.....	97
<b>Figure 5.3</b> Simulated unfolding time regimes for proteins undergoing reversible two-step denaturation by CE .....	109

## LIST OF TABLES

<b>Table 2.1</b> Thermodynamic and electrokinetic factors influencing polyol analyses by DC-CE .....	37
<b>Table 2.2</b> Thermodynamic and electrokinetic parameters influencing polyol separation with NPBA by DC-CE. ....	47
<b>Table 2.3</b> Experimental variables, ranges and conditions selected in the central composite design <sup>†</sup> for optimization of polyol resolution by DC-CE.....	49
<b>Table 2.4</b> Method validation for single-step analysis of polyols by DC-CE under optimum separation conditions.....	58
<b>Table 3.1</b> Comparison of thermodynamic parameters for conformational stability and relative binding affinity of <i>holo</i> -RI $\alpha$ -cNT by DLE-ACE.....	69
<b>Table 4.1</b> $pK_a$ and $K_b$ values of a series of substituted PBA compounds.....	89

## LIST OF ABBREVIATIONS

$\Delta H$	Enthalpy
$\Delta G_U$	Free energy of protein unfolding
$\Delta\Delta G_U^0$	Difference in free energy of apo/olo protein states
$\Delta G_U^0$	Standard free energy of protein unfolding
$\varepsilon$	Dielectric constant
$\mu^A$	Apparent mobility
$\mu_{ep}^A$	Apparent electrophoretic mobility
$\mu_{eo}$	Electroosmotic mobility
$\mu_{ep,A}, \mu_{ep}$	Electrophoretic mobility
$\mu_{ep,C}$	Electrophoretic mobility of ligand
$\mu_{ep,AC}$	Electrophoretic mobility of complexed analyte
$\mu_{ep,F}$	Mobility of the folded native protein
$\mu_{ep,U}$	Mobility of the unfolded protein
$\eta$	Solution viscosity
$v$	Migration velocity
$v\mu_{ep}^A$	Viscosity corrected apparent mobility of the analyte
$\zeta$	Zeta potential
$AC$	Complexed analyte
$C$	Ligand
$C_m$	Mid-point denaturant concentration for equal fraction of folded and unfolded protein
$D$	Diffusion constant
$E$	Electric field



$f_A$	Fraction of free analyte
$f_F$	Fraction of folded protein
$f_U$	Fraction of unfolded protein
$K_a$	Apparent acid dissociation constant
$K_b$	Binding constant
$K_U$	Unfolding constant
$m$	Cooperativity of unfolding
$N$	Number of theoretical plates
$Q_{eff}$	Effective charge of analyte
$R_H$	Hydrodynamic radius
$R_s$	Resolution
AKAP's	A-kinase anchoring proteins
BGE	Background electrolyte
cAPK	cAMP dependent protein kinase A
CCD	Central composite design
CE	Capillary electrophoresis
cNT	Cyclic Nucleotide
CV	Coefficient of variation
DC-CE	Dynamic complexation-capillary electrophoresis
DLE-ACE	Dynamic ligand exchange-affinity capillary electrophoresis
EOF	Electroosmotic flow
ESI-MS	Electrospray ionization-mass spectrometry
Gal	Galactitol
GC	Gas chromatography
HPLC	High performance liquid chromatography
HTS	High throughput screening
LC	Liquid chromatography
LIF	Laser-induced fluorescence

LINF	Laser-induced native fluorescence
LOD	Limit of detection
Man	Mannitol
MS	Mass spectrometry
NMR	Nuclear magnetic resonance
NPBA	3-Nitrophenylboronic acid
PBA	Phenylboronic acid
PKA	Protein kinase A
R	Regulatory subunit
R1 $\alpha$ -PKA	Regulatory subunit of protein kinase A
RPI	Ribose-5-Phosphate isomerase
SDS	Sodium dodecylsulphate
Sor	Sorbitol
TALDO	Deficiency of Transaldolase
Trp	Tryptophan

# **CHAPTER I**

## **1. Background**

## 1.1 Introduction

Electrophoresis is a microseparation technique based upon the differential migration of ions in solution under an external electric field. While the term “electrophoresis” was coined in 1909 by Michaelis,<sup>1</sup> it was the pioneering experiments of Tiselius in 1937<sup>2</sup> that first demonstrated the separation of serum proteins (*e.g.* albumin and globulins) by “moving boundary electrophoresis”; this provided the first example of the potential use of electrophoretic separations for biologically relevant molecules. In 1967 Hjerten<sup>3</sup> showed that it was possible to carry out separations in a 300  $\mu\text{m}$  glass tube and to detect the separated compounds by ultraviolet absorbance. Although other researchers used electrophoresis in glass and Teflon tubes, CE did not become popular until 1981 when Jorgenson and Lukacs published their seminal work in which they demonstrated the high efficiency of separation of dansylated amino acids using micron-sized fused silica capillaries in conjunction with laser-induced fluorescence (LIF) detection.<sup>4</sup> Later in 1984, Terabe demonstrated the use of micelles added to the running buffer solution in order to resolve a mixture of neutral compounds.<sup>5</sup> These pioneering studies highlight the versatility of CE separations to resolve diverse classes of analytes, including ionic and neutral species as well as enantiomers, by exploiting differential

intermolecular interactions during electromigration via changes in composition of the background electrolyte (BGE).

## **1.2 CE: A versatile technique?**

The field of separation science has been dominated mainly by two major instrumental formats: gas chromatography (GC) and high performance liquid chromatography (HPLC). Even though CE has met a lot of success in the last 25 years, GC and HPLC are still extensively used; however, CE has several distinct advantages, such as its simplicity and applicability to separate widely different compounds ranging from inorganic ions, metabolites, and high molecular weight biomolecules under a single instrumental format with an open tubular capillary. This cannot be said about any of the other separation technique. In addition, CE has the highest resolving power of any liquid separation technique due to its fast analysis times and unique flat plug flow profile that minimizes band broadening. CE can also be configured as a high-throughput screening platform, reflected by its critical role in the early completion of the Human Genome Project.<sup>6</sup>

An ideal separation technique can be defined as one that can be applied to the separation, detection, and quantification of a wide variety of

mixtures. It should have high resolving power while being fast and reproducible. Also, separations must be automated, simple and economical to operate, as well as environmentally friendly while being multidimensional so that it can be applied for to complex real-world samples with minimal sample handling. Not one of the existing separation techniques fully meets the above criteria; however, CE comes very close, as will be demonstrated in the two major projects of this thesis.

CE is fast, simple to use, can be automated, and provides quantitative data when coupled to various detector formats, such as UV absorbance, LIF, mass spectrometry (MS) and nuclear magnetic resonance (NMR). It should be noted that CE is mainly an analytical and not a preparative technique. However, the amount of material needed for a CE experiment is very small, typically nanoliters of sample and microliters of buffer, whereas other separation techniques (*e.g.* HPLC) often require microliters of sample and milliliters of solvent. The resulting CE waste, mostly an aqueous buffer with a small percentage of an organic modifier, is relatively safe and can be discarded without any danger to the environment. This is not true when HPLC is used where large amounts of organic solvent waste are generated.

### 1.3 Electrophoresis in a capillary?

Historically, electrophoresis was performed in gel, paper or other support medium in the form of a bed, or slab. However, this approach was limited by the incomplete separation of proteins, the relatively large sample volumes needed and the requirement of low electrical field strengths due to detrimental ion conduction causing Joule heating. The use of narrow fused-silica capillaries as a micro-scale electromigration channel for the separation of various ionic analytes, not only provides a unique approach to separation, but also offers several advantages over conventional solid supports used in classical electrophoresis. In particular, the physical characteristics of narrow-bore fused-silica capillaries make them ideal for electrophoresis.

Fused-silica capillaries employed in CE typically have an internal diameter (*i.d.*) of 20-100  $\mu\text{m}$ , lengths of 20-100 cm, and are externally coated with a thin layer of polyimide, which imparts flexibility to a capillary that would otherwise be very fragile. The high surface-to-volume ratio of capillaries with these dimensions allows for very efficient dissipation of heat generated by the migration of ions in solution. In addition to the high thermal dispersion, the use of capillaries for electrophoresis is associated with several other advantages. With typical electrophoresis capillaries, the small dimensions require microlitre volumes of aqueous buffer solution

(e.g. 0.2-1 mL) with sample volumes introduced into the capillary in the nanoliter range ( $\approx 10$  nL). As a result, as little as a 5  $\mu$ L of sample will suffice for repetitive analysis on some commercial CE instruments. Considering the small reagent (buffer) and sample requirements, as well as the rapid analysis times with the application of high voltages, it is clear why CE has been applied to a diverse number of challenging analytical problems across various disciplines ranging from the determination of priority pollutants in environmental samples,<sup>7</sup> to the analysis of the components of a single cell<sup>8</sup>, and the screening of abnormal proteins or DNA fragments indicative of disease or specific typing of an individual.<sup>1,9</sup>

#### 1.4 Instrumentation in CE analysis

A schematic of a CE instrument is depicted in **Figure 1.1**. The basic components include a high voltage power supply (0-30 kV), a polyimide-coated narrow-bore fused-silica capillary, two buffer reservoirs that can accommodate both the capillary and platinum electrodes connected to the power supply, and an on-line photometric detector, such as UV absorbance or LIF.

To perform a CE separation, the capillary is first filled with an appropriate background electrolyte (BGE) and the sample is introduced at the capillary inlet followed by an application of a positive pressure (*i.e.*,



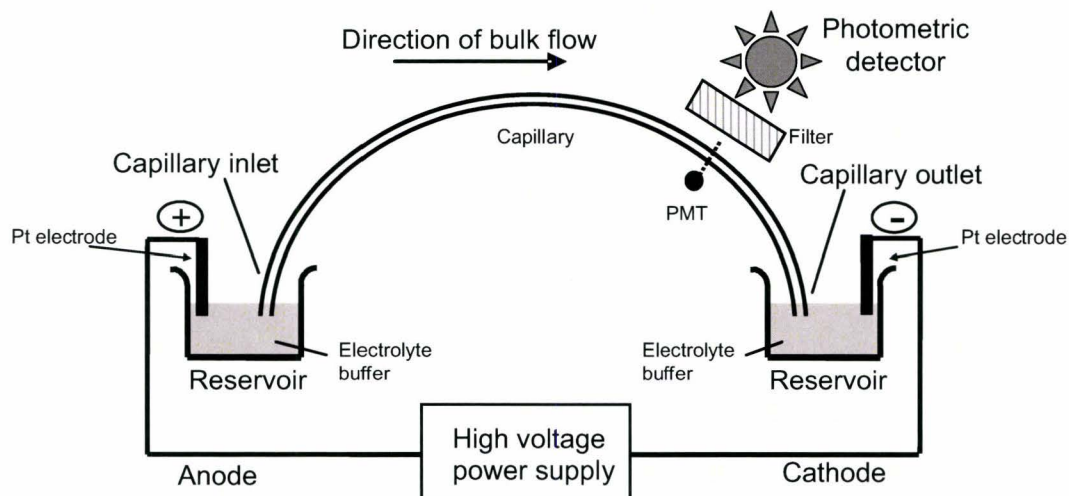


**Figure 1.1** Schematic diagram of a CE instrument with on-line UV absorbance detection. The main components are the temperature-controlled narrow-bore fused-silica capillary, two buffer reservoirs, two platinum electrodes connected to the high power voltage supply, and an on-line photometric detector.

injection) for a fixed period of time. After sample injection, both ends of the capillary and electrodes are placed into buffer reservoirs and up to 30 kV are applied to the system. Intrinsicly charged analytes in the sample plug migrate with a characteristic mobility whose direction and magnitude are determined by their effective charge to size ratio. The analytes migrate past a fixed detector located at the distal end of the capillary, where the signal is collected and stored by a data acquisition system.

### 1.5 Electrophoretic mobility and electroosmotic flow

In CE under “normal” polarity conditions [positive inlet, negative

outlet], analytes are resolved according to their intrinsic electrophoretic mobilities ( $\mu_{ep}$ ) and migrate past a detector as discrete analyte zones. The fact that, under appropriate conditions, all species (net positive, net negative or neutral) can reach the detector indicates that a force other than  $\mu_{ep}$  is involved. If the applied field were the only force acting on the ions, positive ions would arrive at the detector while neutral components would remain static (*i.e.*, at the inlet), whereas anions would be driven away from the detector out of the capillary inlet. Fortunately, there is another intrinsic electrokinetic phenomenon in CE referred to as the “electroosmotic flow” (EOF) (refer to *section 1.7* below), which drives the movement of all components in the capillary towards a fixed detector when under an applied electric field. Therefore, the apparent mobility of a given analyte ( $\mu^A$ ) is due to the superimposition of two major electrokinetic processes, namely the analyte electrophoretic mobility ( $\mu_{ep,A}$ ) and the electroosmotic mobility ( $\mu_{eo}$ ) or EOF. The former term is a fundamental physicochemical property of a solute, which determines overall selectivity, whereas the latter term is dependant on the composition of the buffer and capillary surface that acts as a natural electrokinetic pumping mechanism for fluid transport.

## 1.6 Electrophoretic mobility

For each ion, its migration velocity ( $v$ ) is a result of steady-state equilibrium between the electric force  $F$ , which is exerted by the electric field ( $E$ ), and viscous drag force due to the solution. Neutral species are unresolved in CE except if an ionic additive is included to the BGE. The influence of these factors on  $\mu_{ep,A}$  for a spherically charged analyte is described by Debye-Huckel-Henry theory:

$$\mu_{ep,A} = \frac{v}{E} = \frac{Q_{eff}}{6\pi\eta R_H} \quad (1.1)$$

where,  $Q_{eff}$  is the effective charge of the analyte,  $\eta$  is the viscosity of the buffer, and  $R_H$  is the hydrodynamic radius. **Equation 1.1** highlights the fact that selectivity in CE is based on differences in the direction and magnitude of  $\mu_{ep,A}$ , which is reflected by the effective charge to size ratio of an analyte. For instance, small highly charged anions will have a large negative  $\mu_{ep,A}$ , whereas large minimally charged cations will have low positive  $\mu_{ep,A}$ . In the case of neutral analytes with no intrinsic mobility, they will co-migrate with the EOF. Analytes that have similar chemical properties (e.g., enantiomers) typically have the same  $\mu_{ep,A}$  in an achiral buffer environment. One of the major advantages of CE is that the intrinsic analyte mobility can be readily modified by changes in the composition of

the BGE, such as buffer type, pH, and ionic strength, as well as the use of specific additives, such as cyclodextrins.<sup>10</sup> Buffer pH is an important parameter for improving resolution in CE that is especially relevant for weakly ionic analytes, such as amino acids. The buffer serves multiple functions in CE, such as controlling the degree of analyte ionization (*i.e.*,  $Q_{eff}$ ), resisting changes in buffer pH during separation due to water electrolysis, as well as providing charged carriers to complete the electric circuit. It is important to note that  $\mu_{ep,A}$  represents an intrinsic physicochemical property of an analyte under defined conditions, such as temperature, solution viscosity and buffer pH. Changes in the measured analyte mobility by CE can be used in the determination of fundamental physicochemical properties of analytes, such as  $pK_a$ ,<sup>11,12</sup> diffusion constant<sup>13</sup> and binding constant.<sup>14</sup>

## 1.7 Electroosmotic flow (EOF)

The EOF was first identified in the late 1800s when Helmholtz conducted experiments involving the application of an electric field to a horizontal glass tube containing an aqueous salt solution. Curious about the ionic character of the inner wall and the movement of ions, he found that the silica imparted a layer of negative charge to the inner surface of

the tube, which under an applied electric field led the net movement of fluid toward the cathode. More than a century later, this phenomenon still plays a fundamental role in CE analysis. As a continuation of the pioneering work of Helmholtz, the basic principles governing EOF have been investigated extensively. As shown by the expanded region of the inner wall of a capillary in **Figure 1.2**, the ionized silanol groups (SiOH) of the capillary wall electrostatically adsorb cations in the BGE. Buffer pH will determine the fraction of the silanol groups that will be ionized; understanding the amorphous nature of silica and the  $pK_a$  range ( $pK_a \sim 6.5$ ) associated with the various types of silanol groups is key. The ionic layer that is formed (e.g.,  $\text{Na}^+$ ) has a positive charge density that decreases exponentially as the distance from the wall increases. The double layer formed closest to the capillary surface is termed the “Inner Helmholtz” or “Stern” layer, which represents immobile adsorbed ions. A more diffuse layer formed distal to the Stern Layer is termed the “Outer Helmholtz Plane” (OHP) or the diffuse electric double layer, which is fundamental to the generation of the EOF.<sup>15</sup>

Under an applied electric field, solvated cations in the diffuse double layer migrate in the direction of the cathode carrying waters of hydration with them. Because of the cohesive nature of the hydrogen bonding of the water molecules in the bulk solution, the entire buffer solution is pulled

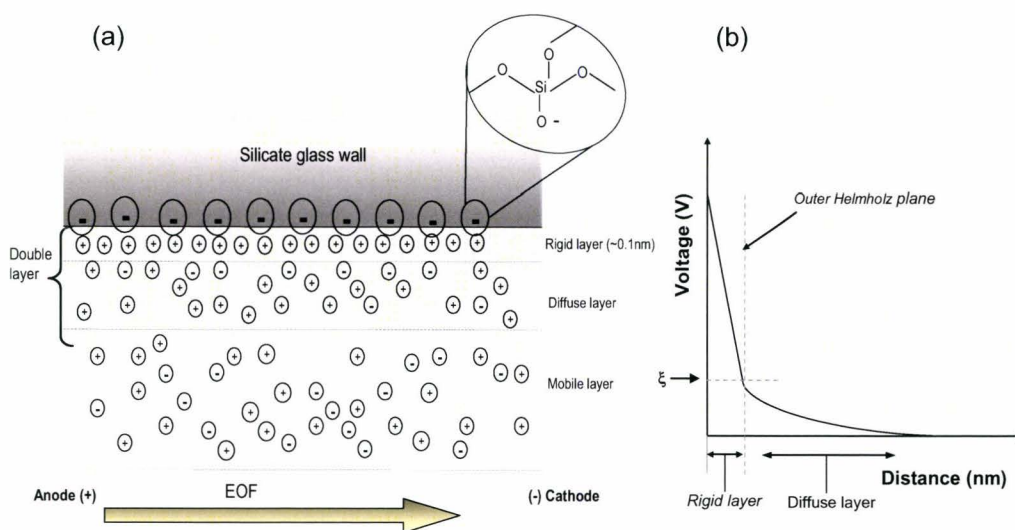


**Figure 1.2** Debye-Hueckel-Stern model of the electric double layer highlighting (a) the diffuse double layer and (b)  $\zeta$  (zeta potential) is the potential at the slipping plane between the rigid and diffuse layers, which decreases exponentially away from the surface of the capillary.

toward the cathode.<sup>1</sup> This EOF or “bulk flow” acts as a natural electrokinetic pumping mechanism to propel all molecules (cationic, neutral and anionic) toward the detector with selectivity ultimately being determined by differences in  $\mu_{ep}$ . Provided that the EOF is moderate but not too strong, adequate residence times of analytes in CE allow for their resolution. However, if the EOF is too weak, there are long migration times and excessive diffusion of the analyte zones resulting in band broadening and poor resolution.

The EOF is a natural fluid transport mechanism that plays an important role in most CE separations. However, under strongly acidic conditions ( $\text{pH} < 2$ ), the silanol surface of the capillary is primarily protonated (neutral), resulting in suppressed EOF. Thus, the pH of the buffer is the major factor that controls the fraction of silanol ionization, which impacts the magnitude of the EOF. In addition, the ionic strength of the BGE can modulate the effective charge at the surface of the capillary. The zeta potential ( $\zeta$ ) is defined as the potential at the slipping plane between the rigid and diffuse double layer, which decreases exponentially away from the surface of the capillary. Upon application of an external voltage perpendicular to  $\zeta$ , there is a net migration of cations in the diffuse double layer towards the cathode. Thus, the EOF propels all analytes (cationic, anionic and neutral) towards the detector. The EOF is defined along planar surfaces by the following **Equation 1.2**:

$$\mu_{eo} = \frac{\varepsilon\zeta}{4\pi\eta} \quad (1.2)$$

where,  $\varepsilon$  is the dielectric constant of the BGE,  $\zeta$  is the potential across the diffuse layer and  $\eta$  is the viscosity of the solution.  $\zeta$  is proportional to the charge density near the surface of the capillary wall, which depends on the pH and ionic strength of the buffer solution. In general, alkaline buffer solutions of low ionic strength generate a high  $\zeta$  and strong EOF.

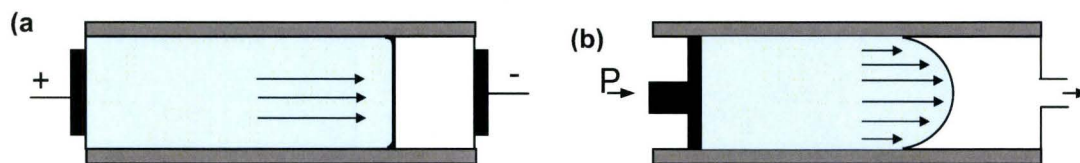


**Figure 1.3** (a) A nearly flat electrokinetic EOF profile in CE which minimizes band broadening and (b) a parabolic flow profile of a pressure-driven pump in HPLC.

Under most conditions in CE ( $\text{pH} > 4$ ), the magnitude of the EOF is greater in magnitude than  $\mu_{ep,A}$ . An important feature of the EOF is that it has a near flat profile as shown in **Figure 1.3 (a)**. The flat profile is attributed to the fact that the charge on the capillary is uniformly distributed so there is no pressure drop, hence generating a uniform flow velocity across the capillary, except at the capillary surface. In contrast, differential frictional forces in HPLC using an external pump cause a pressure drop across the capillary resulting in a parabolic flow profile, as shown in **Figure 1.3 (b)**. The flat profile of the EOF in CE is important because it minimizes longitudinal band broadening, leading to higher separation efficiency (e.g., plate numbers  $> 10^5$ ) and sharper analyte peaks with improved resolution, often over 10-fold greater than HPLC separations.

### 1.8 Apparent mobility

The apparent electrophoretic mobility of an analyte ( $\mu_{ep}^A$ ) is the vector



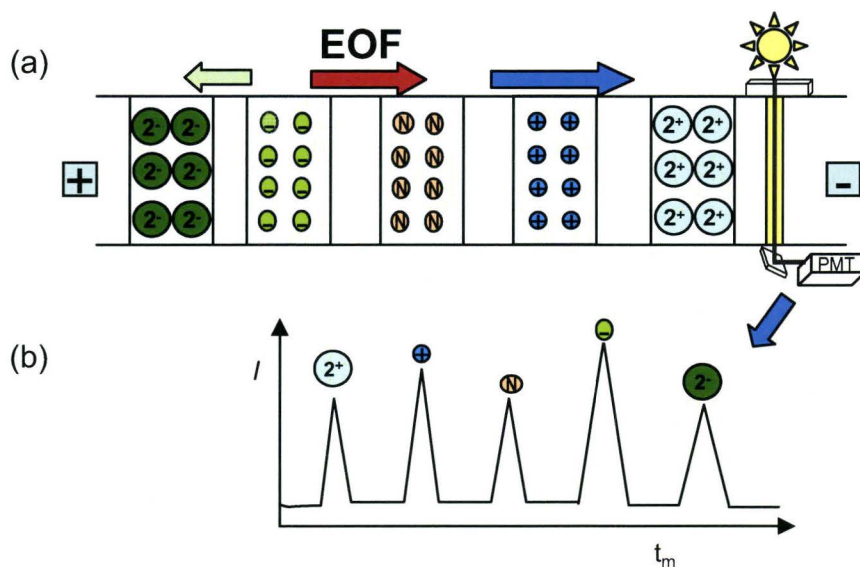


**Figure 1.4** Schematic showing (a) the migration order of the components of a hypothetical mixture of analytes based on their  $\mu_{ep,A}$  by CE, and (b) the electropherogram generated by monitoring the signal intensity as a function of time.

sum of  $\mu_{ep,A}$  and  $\mu_{eo}$  as described by the following equation:

$$\mu_{ep}^A = \mu_{ep,A} + \mu_{eo} \quad (1.3)$$

A schematic of a typical CE separation involving five different analytes in a mixture, namely cations, anions and neutral species is depicted in **Figure 1.4**. The capillary is first rinsed and filled with BGE using an external high pressure, followed by a short hydrodynamic injection of the sample mixture at the inlet end of the capillary. Upon application of the voltage, the sample plug is transported by the EOF while discrete analyte zones are separated based on differences in their intrinsic  $\mu_{ep,A}$ , as shown in **Figure 1.4 (a)**. Note that the relative migration order is based on the

effective charge state of the analyte, in the order of cations, neutrals (co-migrate with EOF) and anions, and that zonal separation of analytes continues until the EOF transports all species across a fixed detector window located at the cathodic end of the capillary.

The monitoring of the signal (*e.g.*, absorbance, fluorescence) as a function of time during separation generates an electropherogram as shown in **Figure 1.4 (b)**, where the apparent analyte migration time is reflected by the superimposition of both EOF and  $\mu_{ep,A}$ . The analyte mobility  $\mu_{ep,A}$  can then be calculated from the apparent migration times of charged and neutral analytes in an electropherogram by re-arranging **equation 1.3** to the following:

$$\mu_{ep,A} = \frac{L_c L_d}{V} \left( \frac{1}{t_A} - \frac{1}{t_{eo}} \right) \quad (1.4)$$

where,  $L_c$  is the total capillary length,  $L_d$  is the effective capillary length to detector,  $V$  is the applied voltage,  $t_A$  is the apparent analyte migration time and  $t_{eo}$  is the migration time of a neutral EOF marker. Due to EOF variation, the measured migration times in CE typically have larger variation (CV > 5 %) than HPLC, however this can be minimized by appropriate capillary pre-rinsing and storage techniques, as well as using internal standards for normalization. However, with the use of a neutral

EOF marker (e.g., caffeine),  $\mu_{ep,A}$  can be measured very precisely (CV < 1%) using commercial CE instruments with thermostatic control. Thus, most separation scientists prefer to consider  $\mu_{ep,A}$  rather than migration times as a reliable parameter to characterize CE separations.

### 1.9 Separation efficiency and resolution

Column efficiency in CE is gauged by the number of theoretical plates ( $N$ ) generated by the column. The theoretical expression for  $N$  has its origin from chromatographic theory and is defined as the following:<sup>4</sup>

$$N = \frac{\mu V}{2D} \quad (1.5)$$

where  $\mu$  is the net ion mobility,  $V$  is the applied voltage and  $D$  is the diffusion constant. The assumption inherent in this expression is that solute diffusion is the only zone broadening mechanism. In practice, many experimental parameters such as sample introduction, analyte adsorption to capillary wall and Joule heating can adversely affect column efficiency. According to **equation 1.5**, the number of theoretical plates ( $N$ ) increases with increasing voltage. Therefore, maximum column efficiency is attained at the highest possible applied voltage.

By using the width at half-height ( $w_{1/2}$ ) of a Gaussian peak, a simplified equation for the efficiency is then obtained:

$$N = 5.54 \left( \frac{t_A}{w_{1/2}} \right)^2 \quad (1.6)$$

where,  $t_A$  is the apparent migration time of the analyte. The characteristics of a Gaussian profile describe the peak maximum and the peak width. The peak maximum is dependent on initial concentration of solute, while the width depends on the length of time from initial conditions (*i.e.*, from introduction of sample into the system) and the diffusion constant,  $D$ .

The resolution ( $R_s$ ) equation in CE is also derived from the same basic principles as chromatography and is given by the following expression:

$$R_s = \frac{1}{4} \frac{(\Delta\mu_{ep}^A) N^{1/2}}{\mu_{avg}} \quad (1.7)$$

where,  $\Delta\mu_{ep}^A$  is the relative mobility difference of the two solutes being separated, and  $\mu_{avg}$  is the average mobility of the two analytes. Since  $R_s$  increases with the applied electric field strength, it is desirable to use high voltages to achieve high resolution separations, as well as to maximize the difference in the net mobility of the analytes. The later feature can be achieved by selecting an appropriate additive, adjusting the additive concentration, or even using more than one additive in the CE system. In

addition, **equation 1.7** permits independent assessment of the two factors that affect overall resolution, namely selectivity and efficiency. The selectivity is reflected by the mobility differences of the analyte(s) ( $\Delta\mu_{ep}^A$ ), while the efficiency of the separation process is indicated by  $N$ . When the column efficiency is the same, longer migration times give better  $R_s$  because the difference in the  $\mu_{ep}^A$  can contribute longer to the differential migration.

### 1.10 Dynamic complexation using additives in CE

Two seemingly unrelated areas of separation science, chromatography and electrophoresis, were united when Terabe *et al.*<sup>16,17</sup> first introduced micellar additives into the BGE in CE for the resolution of both charged and neutral analytes. In this case, micelles function as moving pseudo-stationary phases that can partition with specific analytes during electromigration, a separation mode referred to as micellar electrokinetic chromatography (MEKC). Unlike conventional chromatography, the concentration and specific type of additive(s) (*e.g.*, surfactant, cyclodextrin, metal ion, protein *etc.*) can be readily modified in free solution by CE without stationary phase preparation and column packing. The migration behavior of an analyte in CE is thus controlled by

both electric field and equilibria processes operative in the system which can influence  $\mu_{ep}^A$ .<sup>18</sup>

### 1.10.1 Theory

The selectivity required to resolve species *A* from *B* in an additive-free CE-system is determined by differences in their effective charge to size ratio or  $\mu_{ep}^A$ . If the two free mobilities are the same, an additive can be used in the BGE to form dynamic complexes of different stabilities with two or more analytes. Thus, differential binding affinity and complex mobility can impact  $\mu_{ep}^A$  for analytes to allow for their resolution. As with other separation techniques, CE can be a useful tool for studying biomolecular interactions. CE binding studies involve measuring the change in solute  $\mu_{ep}^A$  caused by the addition of a discrete additive to the BGE, where mobility changes are due exclusively to the association of the solute with additive during electromigration.

Equilibrium constants for molecular association can be measured using a variety of experimental techniques including spectroscopy, calorimetry,<sup>19</sup> potentiometry<sup>20</sup> and reaction kinetics.<sup>21</sup> In order to estimate a binding constant, the system response must be different for the complexed and free analyte. The response of the experimental system is

commonly measured successively using different substrate or ligand concentrations while maintaining a constant solute concentration. The system response can be related to the relative concentrations of associated and free analyte, to the binding constant and other physical properties inherent to the molecular complex and free analyte, such as extinction coefficients in spectrophotometry, chemical shifts in NMR, retention factors in chromatography, and mobilities in electrophoresis.

The most common method used to estimate binding constants by CE involves measuring the change in mobility of a solute (e.g., ligand) in a BGE containing increasing concentrations of additive (*i.e.*, receptor). There are several requirements that must be met in order to use CE in this manner to estimate binding constants. First, the solute must undergo a change in  $\mu_{ep}^A$  upon complexation. Thus, either the solute or the ligand must be intrinsically charged under the experimental conditions in order to satisfy these criteria. Second, the equilibrium time scale must be faster than the CE separation time scale. The third requirement is that sufficient concentrations of both free ligand and ligand/solute complex should be present.

In CE, the theoretical description of binding is derived from fundamental electrophoretic relationships that consider a system containing a solute *A*, which reversibly binds to a complexing agent, *C*

based on a 1:1 dynamic complexation model:



where  $A$  is the analyte,  $C$  is the additive or complexing agent (*i.e.*, surfactant, boronic acid, protein, etc.) and  $AC$  is the complex. Since the equilibrium between  $A$  and  $C$  is established in the capillary, the apparent mobility of analyte  $\mu_{ep}^A$  thus depends on the magnitude of the binding constant and complex mobility  $\mu_{ep,AC}$ .

The binding constant  $K_b$  for a dynamic 1:1 equilibrium reaction is described by the following equation:

$$K_b = \frac{[AC]}{[A][C]} \quad (1.9)$$

where  $[AC]$  is the complex concentration,  $[A]$  is the analyte concentration and  $[C]$  is the concentration of additive.

The retention factor  $k'$ , also called the mass distribution coefficient, is defined as the ratio of the amount of complex to the amount of free analyte. Because the additive and the analyte are in the same solution,  $k'$  is defined as:

$$k' = \frac{AC}{A} = \frac{[AC]}{[A]} = K_b[C] \quad (1.10)$$

In CE, the retention factor is proportional to the additive concentration which can be independently controlled unlike stationary phase column



packing in HPLC. The fraction of the free analyte  $f_A$  is defined as  $[A]/[A]_0$  ( $[A]_0$  is the original analyte concentration). When  $[C]_0$ , the initial additive concentration, is much greater than  $[A]_0$ ,  $[C]$  is equal to  $[C]_0$ . By substituting  $[A]_0$  by  $[A]+[AC]$ , the following expression for  $f_A$  results in:

$$f_A = \frac{1}{1 + K_b[C]} \quad (1.11)$$

Therefore, the apparent electrophoretic mobility of an analyte  $A$  can be expressed by the following equation:

$$\mu_{ep}^A = f_A \mu_{ep,A} + (1 - f_A) \mu_{ep,AC} = \frac{1}{1 + K_b[C]} \mu_{ep,A} + \frac{K_b[C]}{1 + K_b[C]} \mu_{ep,AC} \quad (1.12)$$

Where,  $\mu_{ep,A}$  is the mobility of the free analyte,  $\mu_{ep,AC}$  is the mobility of the complex and  $K_b$  is the apparent binding constant.

**Equation 1.12** is only valid for the ideal situation when changes in additive concentration do not affect the viscosity. In reality, viscosity is often changed with high concentration of additive. A viscosity correction factor  $\nu$ , can be introduced to correct the apparent analyte mobility to an ideal state where the additive concentration approaches zero:

$$\nu \mu_{ep}^A = \frac{1}{1 + K_b[C]} \mu_{ep,A} + \frac{K_b[C]}{1 + K_b[C]} \mu_{ep,AC} \quad (1.13)$$

The correction factor  $\nu$ , is defined as  $\eta/\eta^0$ , where  $\eta$  is the viscosity of the solution and  $\eta^0$  is the viscosity when  $[C]$  is equal to zero. Because of the

increase in viscosity, the value of  $\nu$  is always greater than or equal to one, and the absolute value of the apparent  $\mu_{ep}$  is always smaller than or equal to  $\nu\mu_{ep}^A$ . However, in cases when the analyte is electrically neutral ( $\mu_{ep,A} = 0$ ), **equation 1.13** simplify to the following:

$$\nu\mu_{ep}^A = \frac{K_b[C]}{1 + K_b[C]} \mu_{ep,AC} \quad (1.14)$$

The values of  $K_b$  and  $\mu_{ep,AC}$  can be determined using non-linear regression (1.14), or linear regression (1.15-1.17) when rearranged into one of these transformations:

$$\frac{1}{\nu(\mu^A - \mu_{eo}) - \mu_{ep,A}} = \frac{1}{(\mu_{ep,AC} - \mu_{ep,A})K_b} \frac{1}{[C]} + \frac{1}{(\mu_{ep,AC} - \mu_{ep,A})} \quad (1.15)$$

$$\frac{[C]}{\nu(\mu^A - \mu_{eo}) - \mu_{ep,A}} = \frac{[C]}{(\mu_{ep,AC} - \mu_{ep,A})} + \frac{1}{(\mu_{ep,AC} - \mu_{ep,A})K_b} \quad (1.16)$$

$$\frac{\nu(\mu^A - \mu_{eo}) - \mu_{ep,A}}{[C]} = -K_b(\mu_{ep}^A - \mu_{ep,A}) + K_b(\mu_{ep,AC} - \mu_{ep,A}) \quad (1.17)$$

These equations relate the experimentally measured apparent analyte as a function of ligand concentration ( $[C]$ ) in order to derive the two thermodynamic and electrokinetic parameters that impact separation selectivity, namely binding constant ( $K_b$ ), and complex mobility ( $\mu_{ep,AC}$ ). Plots made according to them have acquired different names, but can generally be referred to as double reciprocal (1.15), y-reciprocal (1.16)

and x-reciprocal (1.17). For example, when the double reciprocal (1.15) is used, plotting  $[1/v(\mu^A - \mu_{eo}) - \mu_{ep,A}]$  vs.  $1/[C]$  should give a straight line from where the value of  $K_b$  is then obtained by dividing the intercept by the slope of the linear fitted line.<sup>18,22,23</sup>

### 1.11 Research Objectives

Despite the wide interest in development of high-throughput screening platforms for drug discovery or disease prognosis, little emphasis has been placed on enhancing “pre-analysis steps” that are often the most crucial component determining the overall performance of an assay. Off-line sample pretreatment protocols for complex biological samples are often time-consuming and not amenable for automation, such as sample preconcentration, chemical labeling, desalting, as well as protein purification. The major goal of this thesis is the development of a single-step analytical platform based on CE for targeted metabolites that integrate several different sample pretreatment processes during separation. In addition, CE will also be used as a biophysical technique for characterization of thermodynamic parameters involving covalent or non-covalent interactions.

Two distinct projects have been investigated in this thesis that illustrate the concept of integrating sample pretreatment with chemical

analysis based on dynamic complexation-capillary electrophoresis (DC-CE), namely boronic acid-polyol and protein-cyclic nucleotide interactions. In the first project, detailed in **Chapter 2**, 3-nitrophenylboronic acid (NPBA) was used as an electrokinetic probe for the dynamic complexation of three polyols, namely sorbitol, galactitol and mannitol. A design of experiment based on a central composite design (CCD) was carried out in order to screen and optimize the most important experimental variables that maximize polyol resolution in DC-CE. A binding study was then performed to measure binding constants and complex mobilities of hexitols using NPBA that influenced their resolution. In the second project, detailed in **Chapter 3**, the characterization of the unfolding dynamics of a recombinant regulatory subunit ( $R\alpha$ ) of cAMP-dependant protein kinase (cAPK) was examined by CE with dual channel laser-induced native fluorescence detection (CE-DC-LINF). Electrophoretic separation of the  $R\alpha$ -cAMP complex, in-capillary generation of the cAMP-stripped *apo*- $R\alpha$  and cyclic nucleotide exchanged *holo*- $R\alpha$  states, as well as dynamic  $R\alpha$  unfolding in urea was carried out directly in-capillary during electromigration by dynamic ligand-exchange-affinity capillary electrophoresis (DLE-ACE), which allowed for assessment of the conformational stability of  $R\alpha$  and its relative binding affinity to different cyclic nucleotide analogues.

## 1.12 References

---

- 1 Handbook of capillary and microchip electrophoresis and associated microtechniques. Edited by J.P. Landers. CRC Press, Third Edition (2008)
- 2 Tiselius A., *Trans. Faraday Soc.* **33** (1937) 524-531.
- 3 Hjertén S., *Chromat. Rev.* **9** (1967) 122-219.
- 4 Jorgenson J.W., Lukacs K.D., *Anal. Chem.* **53** (1981) 1298-1302.
- 5 Terabe S., Otsuka K., Ichikawa K. et al., *Anal. Chem.* **56** (1984) 111-113.
- 6 Thangadurai S., *Anal. Sci.* **20** (2004) 595-601.
- 7 Andreu V., Blasco C., Pico Y., *Trends in Anal. Chem.* **26** (2007) 534-556.
- 8 Toriello N.M. et al., *PNAS*, **105** (2008) 20173-20178.
- 9 Perez-Carbonero L. et al., *Eur. J. Cancer* **45** (2009) 1485-1493.
- 10 Otsuka K., Terabe S. J., *Chromatogr. A*, **875** (2000), 1-2, 163-178.
- 11 Vcelakova K., Zuscova I., Kenndler E., Gas B., *Electrophoresis* **25** (2004) 309-317.
- 12 Ehala S., Misek J., Stara I., Stary I., Kasicka V., *J.Sep.Sci.* **31** (2008) 2686-2693.
- 13 Slater G.W., Mayer. P, Grossman P.D., *Electrophoresis* **16** (1995) 75-83.
- 14 Almeda S. et al., *Talanta* **78** (2009) 1446-1451.
- 15 Wang J., *Analytical Electrochemistry*. Third Edition. John Wiley & Sons, Inc. (2006).
- 16 Terabe S., Otsuka K., Ichikawa K., Tsuchiya A., Ando T., *Anal. Chem.* **56** (1984) 111-113.
- 17 Terabe S., Ozaki H., Otsuka K., Ando T., *J. Chromatogr.* **332** (1985) 211-217.
- 18 Bowser M., Chen D.D.Y., *Electrophoresis* **19** (1998) 383-387.
- 19 Pierce M.M., Raman C.S., Nall B.T., *Methods* **19** (1999) 213-221.
- 20 Nawaz H., Rauf S. et al. *Anal. Biochem.* **354** (2006) 28-34.
- 21 Selvi P.T., Ashish B., Murthy, G.S., *Curr. Sci.* **82** (2002) 1442-1448.
- 22 Rundlett K.L., Armstrong D.W., *J. Chromatogr. A* **721** (1996) 173-186.
- 23 Rundlett K.L., Armstrong D.W., *Electrophoresis* **18** (1997) 2194-2202.

## **CHAPTER II**

### **2. Electrokinetic Probes for Single-step Screening of Polyol Stereoisomers: The Virtues of Ternary Boronate Ester Complex Formation**

*\*This chapter of thesis is derived from the published manuscript:*

Claire Kaiser, Giselle Seguí-Lines, Jason C. D'Amaral, Adam S. Ptolemy  
and Philip Britz-McKibbin *Chemical Communications*, **2008**, 338-340. DOI:  
10.1039/b714215c

*Reproduced by permission of ©The Royal Society of Chemistry*

## 2.1 Abstract

Electrokinetic probes based on the differential migration of ternary boronate ester complexes permit the selective analysis of micromolar levels of UV-transparent polyol stereoisomers in urine samples via dynamic complexation-capillary electrophoresis that is applicable to single-step screening of in-born errors of sugar metabolism, such as galactosemia.

## 2.2 Introduction

The design of boronic acids as probes for carbohydrates has wide interest in the clinical diagnosis of disorders involving sugar metabolism. To date, several groups have developed various boronic acid structural motifs to enable selective binding of sugars using colorimetric or fluorescence detection.<sup>1</sup> Polyols or sugar alcohols represent important clinical target(s) that have been implicated in neuropathic complications with diabetes, as well as biomarkers for in-born errors of metabolism.<sup>2</sup> However, target selectivity and assay sensitivity have been major limitations of conventional boronic acid probes when applied to sub-mM detection of sugar stereoisomers in complex biological samples. Herein, we introduce a new strategy for enhancing target selectivity when using 3-nitrophenylboronic acid (NPBA) as an electrokinetic probe in dynamic complexation-capillary

electrophoresis (DC-CE). Stereoselective resolution of polyols was achieved based on their differential electromigration behavior with NPBA in phosphate buffer. Direct photometric detection of  $\mu\text{M}$  levels of hexitol stereoisomers in urine samples was also realized via *in-situ* generation of a UV-active anionic ternary boronate ester complex. These features are relevant in newborn screening of galactosemia, where early detection of elevated urinary galactitol<sup>2a,e</sup> is crucial to prevent acute liver cirrhosis, neurological impairment and/or neonatal death, which can be treated by a lactose-free diet.<sup>2d</sup>

### 2.3 Results and Discussion

In this study, NPBA was selected as an electrokinetic probe because of its good water solubility, stronger acidity and useful UV spectral properties due to the presence of an electron-withdrawing *nitro* group relative to phenylboronic acid. In general, boronic acid derivatives with lower  $pK_a$  tend to exhibit higher affinity for sugars, although other variables can impact borate chelation, such as buffer pH, ionic strength and electrolyte type.<sup>3</sup> **Figure 2.1** depicts a dynamic complexation model involving reversible 1:1 covalent interactions of NPBA with neutral polyols in the presence of phosphate under an electric field. Note that several distinct equilibria occur in DC-CE such as the formation of trigonal and



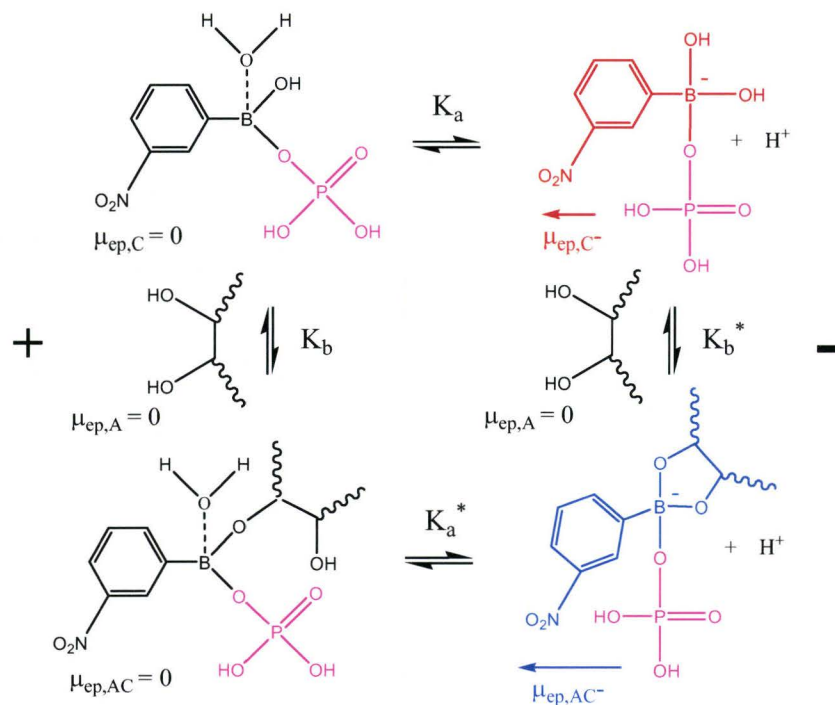


**Figure 2.1** Dynamic complexation model depicting NPBA as an electrokinetic probe for polyols in phosphate buffer by DC-CE. An increase in complex mobility ( $\mu_{ep,AC^-}$  vector arrow) with UV spectral changes for the anionic ternary complex enables the direct analysis of multiple neutral UV-transparent polyol stereoisomers.

tetrahedral boronate ester complexes;<sup>3</sup> however only species that are intrinsically charged contribute to changes in polyol apparent electrophoretic mobility ( $\mu_{ep}^A$ ), such as the NPBA- polyol-phosphate ternary complex. The composition of the buffer can significantly influence the apparent acid dissociation constant ( $K_a$ ) and binding constant ( $K_b$ ) of boronic acids in free solution.<sup>3</sup>

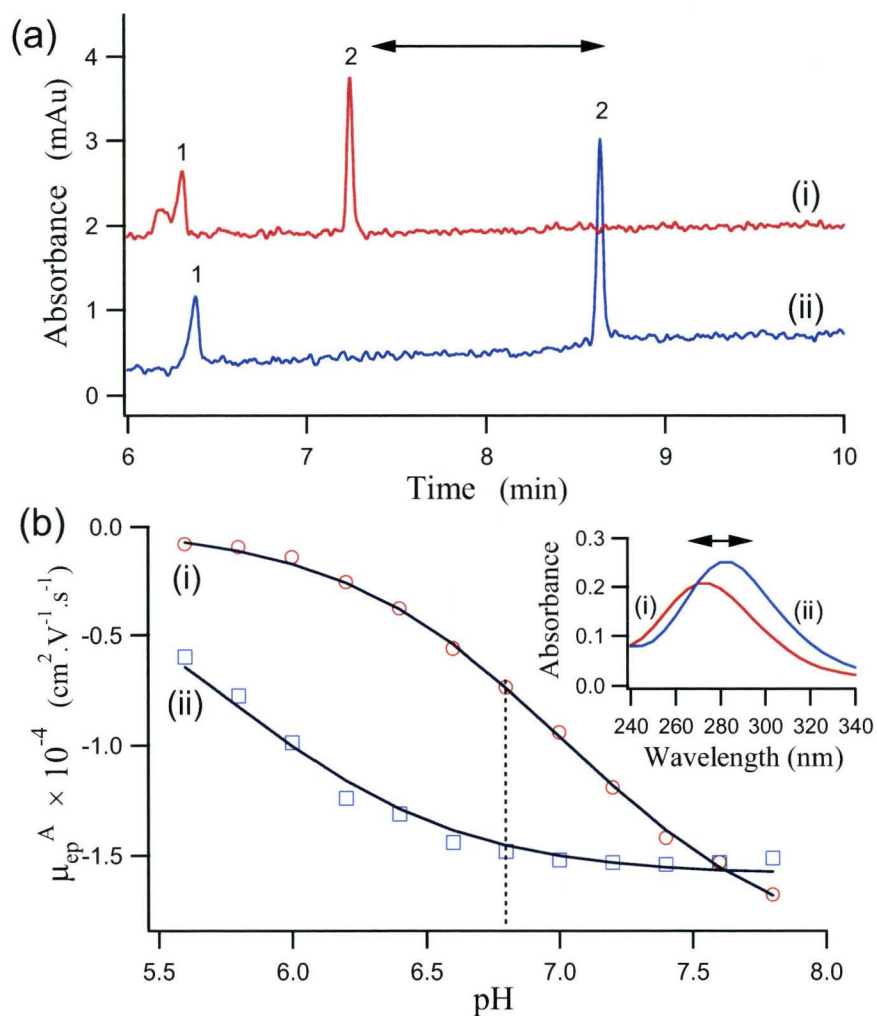


**Figure 2.2** (a) Electropherograms depicting the increase in  $\mu_{ep}^A$  of the NPBA-sorbitol complex (ii) relative to free NPBA (i) where (1) is resorcinol as the neutral EOF marker and (2) NPBA. Conditions: 27 mM phosphate, pH 6.8 with (i) 0 and (ii) 5 mM sorbitol; voltage: 30 kV, capillary length: 86 cm, temperature: 25°C; UV at 280 nm; sample injection: 3 s using 100  $\mu$ M resorcinol and NPBA. (b) Overlay mobility plots for (i) NPBA and (ii) NPBA-sorbitol complex as a function of buffer pH for the  $pK_a$  and  $pK_a$  determination. Inset of (b) highlights a 10 nm red-shift with absorbance enhancement at 280 nm for (ii) NPBA-sorbitol complex relative to (i) free NPBA, where  $\Delta\epsilon = 2,600 \text{ M}^{-1} \text{ cm}^{-1}$  at 280 nm.

For instance, phosphate has been reported to function as both weak ligand<sup>3b</sup> and proton-exchange catalyst<sup>3d</sup> with boronic acid analogues. **Figure 2.1** highlights that ternary complex formation results in a larger negative complex mobility ( $\mu_{ep,AC^-}$ ) relative to free NPBA ( $\mu_{ep,C^-}$ ), which alters polyol migration behavior based on the affinity of NPBA-polyol interactions. Further evidence of ternary complex formation is provided by CE, UV and NMR experiments.<sup>†</sup>

The apparent mobility, acidity and spectral properties of NPBA were first characterized in phosphate buffer by CE and UV spectroscopy. **Figure 2.2(a)** qualitatively depicts changes in the electromigration of NPBA with the presence of a 50- fold excess of sorbitol in phosphate buffer. It is clear that the apparent negative mobility (*i.e.*, migration time) of NPBA increases significantly with sorbitol chelation despite the increase in hydrodynamic size of the complex. This observation suggests that the fraction of ionization for the NPBA-sorbitol complex increases relative to free NPBA. **Figure 2.2(b)** compares the pH-dependent  $\mu_{ep}^A$  changes of NPBA with 0 or 5 mM sorbitol, which allowed for assessment of the apparent  $pK_a$  of NPBA and NPBA- sorbitol species by non-linear regression.<sup>†</sup>

It was determined that sorbitol complexation with NPBA reduced its apparent  $pK_a$  by 1.2 pH units from  $pK_a = (7.0 \pm 0.2)$  to  $pK_a^* = (5.8 \pm 0.4)$ ,

which resulted in longer migration times for the ternary complex. A similar enhancement in the acidity of phenylboronic acid-diol complexes also been reported by other groups,<sup>3</sup> which has been used as a mode for detection.<sup>1b</sup> NPBA chelation with sorbitol also induced a significant bathochromic shift with hyperchromic effect as shown in the inset of **Figure 2.2(b)**, which provided a simple mechanism for the direct photometric detection of UV-transparent polyols. For instance, there was a red-shift of about 10 nm for the NPBA-sorbitol complex relative to free NPBA along with an increase in its molar absorptivity ( $\Delta\epsilon$ ) of  $2,600 \text{ M}^{-1}\text{cm}^{-1}$  at 280 nm. It was observed that the magnitude of the spectral changes for NPBA was dependent on both the concentration of sorbitol and phosphate in solution, which influence the fraction of ternary complex formed.

**Figure 2.3** depicts a series of electropherograms at increasing [NPBA] that highlights the analysis of a 100  $\mu\text{M}$  polyol mixture with UV detection at 280 nm. All samples also contained catechol and resorcinol, which were used as an internal standard and neutral electroosmotic flow marker (EOF), respectively. At 0 mM NPBA, all analytes are neutral and co-migrate with the EOF; however only catechol and resorcinol are responsive at this wavelength. **Figure 2.3(a)ii** demonstrates that the addition of 3 mM NPBA in phosphate buffer resulted in the separation and detection of anionic ternary complexes at longer migration times except

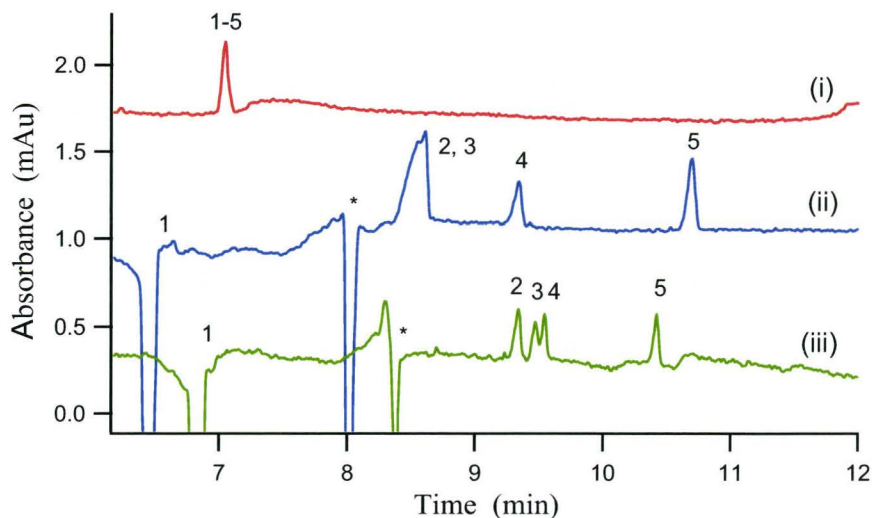


**Figure 2.3** Electropherogram overlay depicting the impact of increasing [NPBA] in phosphate for single-step analysis of polyols by DC-CE. Buffer conditions: 27 mM phosphate, pH 6.8 with (i) 0, (iii) 3 and (iii) 12 mM NPBA. All other conditions as in Fig. 2.2. Peak numbering in plots correspond to 100  $\mu$ M of (1) resorcinol/EOF, (2) mannitol, (3) galactitol, (4) sorbitol and (5) catechol, where \* represents the NPBA system peak.

resorcinol due to its 1,3-dihydroxy configuration. All polyols were partially resolved when using 12 mM NPBA as depicted in **Figure 2.3(iii)**. The use of NPBA generated two large negative system peaks in all electropherograms, the first one corresponding to the EOF and the second zone associated with free NPBA due to the injection of a UV-transparent water plug in the sample. A 2-level/3-factor central composite design was also performed in this study, which revealed that 27 mM phosphate, pH 6.8 at 25°C was the optimum condition to achieve maximum polyol resolution. Overall, buffer pH was the most significant variable impacting

polyol resolution, whereas [phosphate] had a major influence on polyol absorbance response.<sup>†</sup>

To date, the majority of sugar sensors based on boronic acids have focused on enhancing binding affinity while tuning selectivity for specific targets, including polyols.<sup>1d</sup> However, DC-CE provides a thermodynamic and electrokinetic mechanism for high efficiency speciation of polyol stereoisomers using boronic acids in free solution. The latter effect is based on differences in  $\mu_{ep,AC^-}$ , which is reflected by the distinct conformational size of the complex. **Table 2.1** summarizes  $K_b$  and  $\mu_{ep,AC^-}$  parameters for polyols under optimum buffer conditions.<sup>†</sup> It is apparent that sorbitol has about a 2.5-fold greater affinity for NPBA relative to either mannitol or galactitol despite minor differences in their stereochemistry. Interestingly, the apparent binding affinity of mannitol was measured to be slightly greater than galactitol despite its shorter migration time. The anomalous mannitol-galactitol migration order in **Figure 2.3** is explained by differences in  $\mu_{ep,AC^-}$ , where galactitol has a larger  $\mu_{ep,AC^-}$  relative to mannitol despite its weaker affinity to NPBA. Thus, at high [NPBA] near complex saturation,  $\mu_{ep,AC^-}$  override minor differences in  $K_b^*$ , such that galactitol migrates after mannitol. The large  $\mu_{ep,AC^-}$  of galactitol

**Table 2.1** Thermodynamic and electrokinetic factors influencing polyol analyses by DC-CE with NPBA in 27 mM phosphate, pH 6.8.

Polyol	$K_b^a$ ( $M^{-1}$ )	$\Delta H^{ob}$ (kJ/mol)	$T\Delta S^{ob}$ (kJ/mol)	$\mu_{ep,AC^-} \times 10^{-4a}$ ( $cm^2/Vs$ )
Mannitol	(497 ± 17)	-(10.4 ± 2.3)	(5.1 ± 2.2)	-(1.68 ± 0.02)
Galactitol	(453 ± 13)	-(10.5 ± 2.5)	(4.8 ± 2.4)	-(1.77 ± 0.02)
Sorbitol	(1255 ± 46)	-(19.4 ± 2.6)	-(1.6 ± 2.6)	-(1.72 ± 0.01)

<sup>a</sup> Parameters determined at 25°C with error  $\pm 1\sigma$ , where the average mobility of free 3-NPBA was  $-(7.36 \pm 0.02) \times 10^{-5} cm^2/Vs$ . <sup>b</sup> Thermodynamic parameters were derived from double reciprocal binding isotherms ( $n = 3$ ) at five temperatures ranging from 20-40°C.

relative to other hexitols suggests a more compact ternary complex with a smaller hydrodynamic size. The temperature-dependence of NPBA-polyol interactions revealed that the driving force for complexation was enthalpy-driven ( $\Delta H^\circ < 0$ ), with NPBA-sorbitol chelation providing the greatest exothermic and lowest entropy change indicative of tridentate complexation behavior.<sup>1f</sup> In contrast, mannitol and galactitol had similar enthalpy yet large positive entropy changes. Thus, electrokinetic factors (*i.e.*,  $\mu_{ep,AC^-}$ ) played a dominant role underlying the mechanism for resolution of mannitol-galactitol, unlike galactitol-sorbitol, where thermodynamic (*i.e.*,  $\Delta H^\circ$ ) factors had a much more decisive impact.

**Figure 2.4** demonstrates single-step screening of micromolar levels of polyols in human urine samples, including the secondary polyol metabolites, galactonic acid and gluconic acid. Recently, a new method

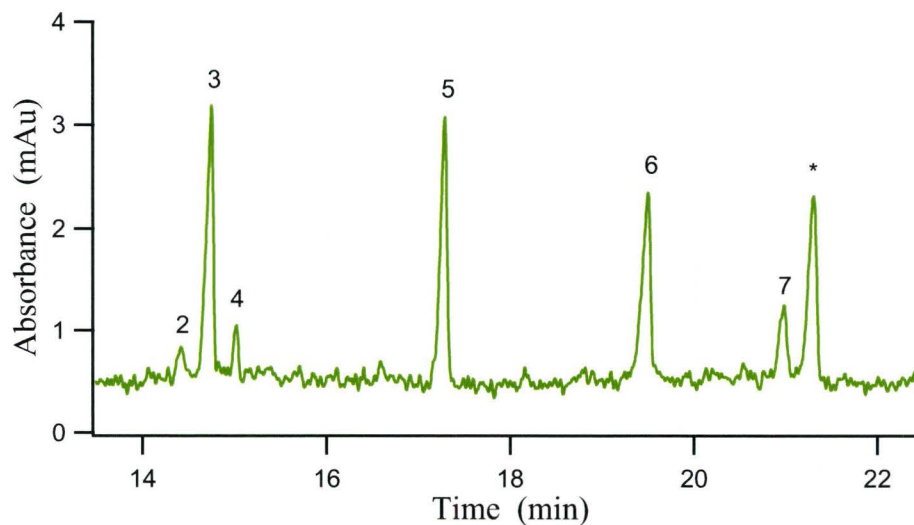


**Figure 2.4** Electropherogram demonstrating single-step screening of urinary polyols after 10-fold dilution in de-ionized water by DC-CE. Spiked healthy urine sample represents a simulated polyol profile associated with galactosemia with elevated galactitol, 3 (400 $\mu$ M) and galactonic acid, 6 (100  $\mu$ M) in the presence of other polyols (40  $\mu$ M) and catechol as IS (200  $\mu$ M). Optimum buffer conditions: 27 mM phosphate, 15 mM NPBA, 1.5 mM MgCl<sub>2</sub>, pH 6.8. All other conditions are similar to Fig. 2.2, except peak numbering, where (6) galactonic acid, (7) gluconic acid and (\*) endogenous uric acid.

for the diagnosis of galactosemia by stable isotope dilution GC-MS,<sup>4b</sup> revealed that galactosemic patients had elevated levels of urinary galactitol and galactonic acid present in about a 4:1 concentration ratio unlike healthy controls. The major disadvantage of GC-MS is the time-consuming off-line sample preparation steps, which includes urease treatment to remove excess uric acid, chemical derivatization for improved volatility of polar polyols, as well as lyophilization and/or liquid extraction sample workup.<sup>2a,4a-c</sup> LC-MS<sup>4d,e</sup> and ion-exchange with pulsed amperometric detection<sup>4f</sup> can reduce the extent of sample cleanup, but



often do not provide adequate resolution of hexitol stereoisomers.<sup>4d</sup> In contrast, **Figure 2.4** highlights direct analysis of urinary polyol stereoisomers that can reliably quantify elevated galactitol and galactonate levels ( $\approx 0.1\text{-}2\text{ mM}$ ) associated with galactosemia<sup>2a,4b</sup> in the presence of uric acid without interferences. The detection limit ( $S/N \approx 3$ ) was determined to be about  $20\ \mu\text{M}$  for polyols by DC-CE, whereas the average polyol recovery ( $n = 10$ ) of a  $100\ \mu\text{M}$  spiked urine sample was about 94%.<sup>†</sup> Method reproducibility ( $n = 10$ ) for spiked urine samples was also assessed in terms of relative peak area and migration time, which provided good precision as reflected by an average CV of 5.2 and 0.3%, respectively.<sup>†</sup>

## 2.4 Conclusions

Electrokinetic probes based on the differential migration of ternary boronate ester complexes offer a unique format for polyol screening, which can be applied for early detection of galactosemia, as well as other disorders of sugar metabolism. Although borate is a widely used alkaline buffer and chelating agent in CE, to the best of our knowledge this is the first report of using phenylboronic acid analogues as probes for the resolution and direct photometric detection of sugars. Notably, our studies revealed the essential role that phosphate plays for enhancing NPBA

absorbance response for polyol detection at low micromolar levels.<sup>†</sup> For instance, the application of other common anionic electrolytes, including carbonate and MES, did not generate a similar UV response for polyols compared to phosphate.<sup>†</sup> Further studies are needed to better understand the role that specific electrolyte conditions can play to improve molecular recognition processes of boronic acids for saccharides. In summary, DC-CE offers a promising microseparation platform detection of sub- $\mu\text{M}$  detection of other classes of sugars using fluorescent boronic acid analogues as electrokinetic probes.

<sup>†</sup>**Electronic supplementary information (ESI) available: Experimental details, central composite design, method validation and ternary complex characterization by CE, UV and NMR. See DOI: [10.1039/b714215c](https://doi.org/10.1039/b714215c)**

## 2.5 References

- 1 (a) T. D. James, M. D. Philips, S. Shinkai in *Boronic Acids in Saccharide Recognition*, RSC Publishing, Cambridge, 2006; (b) J. W. Lee, J.-S. Lee, Y.-T. Chang, *Angew. Chem. Int. Ed.*, 2006, **45**, 6485; (c) R. Badugu, J. R. Lakowicz, C. D. Geddes, *Bioorg. Med. Chem.*, 2005, **13**, 113; (d) J. Zhao, T. D. James, *J. Mater. Chem.*, 2005, **15**, 2896; (e) H. Fang, G. Kaur, B. Wang, *J. Fluorescence*, **14**, 2004, 481; (f) J. C. Norrild, *J. Chem. Soc. Perkin Trans. 2*, 2001, 719.
- 2 (a) C. Yager, S. Wehrli, S. Segal, *Clin. Chimica Acta*, 2006, **366**, 216; (b) E. Jauniaux, J. Hempstock, C. Teng, F. C. Battaglia, G. J. Burton, *J. Clin.*

- Endocrin. Met.*, 2005, **90**, 1171; (c) S. S. M. Chung, E. C. M. Ho, K. S. L. Lam, S. K. Chung, *J. Am. Soc. Nephrol.*, 2003, **14**, S233; (d) S. Schweitzer-Krantz, *Eur. J. Pediatr.*, 2003, **162**, S50; (e) W. W. Wells, T. A. Pittman, T. J. Egan, *J. Biol Chem.*, 1964, **239**, 3192.
- 3 (a) J. Yan, G. Springsteen, S. Deeter, B. Wang, *Tetrahedron*, 2004, **60**, 11205; (b) L. I. Bosch, T. M. Fyles, T. D. James, *Tetrahedron*, 2004, **60**, 11175; (c) G. Springsteen, B. Wang, *Tetrahedron*, 2002, **58**, 5291; (d) R. E. London, S. A. Gabel, *J. Am. Chem. Soc.*, 1994, **116**, 2562.
- 4 (a) J. Lee, B. C. Chung, *J. Chromatogr. B*, 2006, **831**, 126; (b) P. Schadewaldt, H.-W. Hammen, S. Stolpmann, K. Kamalanathan, U. Wendel, *J. Chromatogr. B*, 2004, **801**, 249; (c) H. Yoshii, H. Uchino, C. Ohmura, K. Watanabe, Y. Tanaka, R. Kawamori, *R. Diabetes Res. Clin. Prac.*, 2001, **51**, 115; (d) M. M. C. Wamelink, D. E. C. Smith, C. Jakobs, N. M. Verhoeven, *J. Inherit. Met.*, 2005, **28**, 951; (e) G. Vas, K. Conkrite, W. Amidon, Y. Qian, K. Banki, A. Perl, *J. Mass Spec.*, 2006, **41**, 463; (f) T. R. I. Cataldi, C. Campa, G. E. D. Benedetto, *Fres. J. Anal. Chem.*, 2000, **368**, 739.

## ***Electronic Supplemental Information***

### **2.6 Experimental**

#### **2.6.1 Chemicals and Reagents**

De-ionized water used for buffer and sample preparations was obtained using a Barnstead EASYpure®II LF ultrapure water system (Dubuque, Iowa, USA). Phosphate buffer was prepared using potassium phosphate monobasic purchased from Merck (Darmstadt, Germany). The pH of all run buffer solutions used for CE separations were adjusted by using 1.0 M NaOH. All other analytes and reagents used in this study

were purchased from Sigma-Aldrich (St. Louis, Mo. USA). Individual analyte stock solutions of 10 mM were prepared in de-ionized water and diluted prior to analysis by CE.

### 2.6.2 Apparatus and Conditions

All separations were performed on a P/ACE MDQ CE system equipped with single-channel UV absorbance detector (Beckman-Coulter Inc., Fullerton, CA, USA). Uncoated fused-silica capillaries with 75  $\mu\text{m}$  *i.d.*, 360  $\mu\text{m}$  *o.d.* and 86 cm length with an effective detector length of 76 cm (Polymicro Technologies, Phoenix, USA) were used. A new capillary was first conditioned by high pressure rinsing for 5 min with 0.1 M NaOH, 5 min in de-ionized water and 10 min in background electrolyte. Every separation was then preceded by a 2 min rinse with 0.1 M NaOH and 3 min rinse with background electrolyte prior to sample injection. Hydrodynamic injection of samples were performed at the capillary inlet using a low pressure (0.5 psi or 3.5 kPa) for 3 s. Separations were thermostated at 25°C using an applied voltage of 30 kV with detection at 280 nm unless otherwise stated. All separations were performed in phosphate buffer with different concentrations of NPBA, sorbitol and/or  $\text{MgCl}_2$ . UV spectra were acquired using a Carey 50 spectrophotometer (Varian Inc., Palo Alto, CA, USA) at room temperature using 20  $\mu\text{M}$  NPBA

under different electrolyte conditions. All data processing and linear/non-linear regression was performed using Igor Pro 5.0 (Wavemetrics Inc., Lake Oswego, OR, USA).

### 2.6.3 Central Composite Experimental Design

A two level ( $\pm 1$ )-three factor (*i.e.*,  $2^3$ ) central composite design with six axial ( $\pm 1.7$ ) and five central (0) conditions for a total of 19 experiments were performed to systematically optimize polyol resolution. The three experimental factors examined were buffer pH ( $x_1$ ), capillary phosphate concentration ( $x_2$ ) and temperature ( $x_3$ ) over a range of 6.4-7.8, 3-37 mM and 16.5-33.5°C, respectively. Multiple linear regression of the data matrix was performed by Excel (Microsoft Inc., Redmond, WA, USA). All experimental design studies were performed using a 100  $\mu$ M polyol mixture in the sample with 12 mM NPBA in the background electrolyte in order to acquire sufficient resolution between the two pairs of polyols, namely mannitol-galactitol (2-3) and galactitol-sorbitol (3-4).

### 2.6.4 NMR Spectroscopy

$^{11}\text{B}/^{31}\text{P}$ -NMR studies were performed using a Bruker AV600 MHz equipped with 5 mm multinuclear TBI-Z probe in order to assess NPBA-phosphate-polyol interactions in solution. All NMR samples consisted of 27

mM phosphate, pH 6.8 containing 10% D<sub>2</sub>O with 15 mM NPBA and/or 3 mM sorbitol. Changes in chemical shift as a function of electrolyte composition were reported as relative chemical shift differences ( $\Delta\delta$ ) to either free phosphate or free NPBA in de-ionized water. In most cases, a significant upfield chemical shift change ( $\Delta\delta < 0$ ) was observed due to changes in the electronic environment of <sup>31</sup>P and <sup>11</sup>B nuclei as a result of specific covalent interactions of NPBA with phosphate and/or sorbitol.

### **2.6.5 Human Urine Analysis**

A single-point collection of a morning mid-stream urine sample was provided by a healthy volunteer, which was used within 24 hrs while refrigerated at 4°C. All urine samples were centrifuged for 2 min at 10,000 rpm to remove particulate matter and the supernatant was then diluted 10-fold in de-ionized prior to analysis by DC-CE. Recovery and reproducibility studies were performed by analysis of 100 µM spiked polyols in urine using ten replicate samples ( $n = 10$ ). Analysis of a simulated urinary profile typical for classic galactosemia was also examined to demonstrate adequate selectivity in the presence of elevated galactitol and galactonic acid that have been previously reported to be associated with this metabolic disorder.

## 2.7 Theory

### 2.7.1 $pK_a$ Determination by DC-CE

The pH-dependent  $\mu_{ep}^A$  changes of NPBA as a monoprotic acid in phosphate buffer with the addition of 0 or 5 mM sorbitol allowed for determination of its apparent  $pK_a$  by non-linear regression based on **equation 2.1**:

$$\mu_{ep}^A = \frac{K_a}{K_a + [H^+]} \cdot \mu_{ep,C- / AC-} \quad (2.1)$$

where,  $\mu_{ep}^A$  is the apparent mobility of NPBA or NPBA-sorbitol complex, whereas  $\mu_{ep,C-}$  and  $\mu_{ep,AC-}$  represent the mobility of conjugate base forms of NPBA and NPBA-sorbitol complex, respectively. It was determined that a 1.2 pH unit lower  $pK_a$  for NPBA was induced upon sorbitol complexation reflected by  $pK_a = (7.0 \pm 0.2)$  compared to  $pK_a^* = (5.8 \pm 0.4)$  as depicted in **Figure 2.2(b)** of the manuscript.

### 2.7.2 Binding Constant Determination by DC-CE.

**Figure 2.5** depicts an overlay of double-reciprocal binding isotherms for polyols based on dynamic 1:1 NPBA-polyol interaction in 27 mM phosphate, pH 6.8 using linear regression based on **equation 2.2**:

$$\frac{1}{\mu_{ep}^A} = \frac{1}{\mu_{ep,AC} K_b^*} \cdot \frac{1}{[C]} + \frac{1}{\mu_{ep,AC-}} \quad (2.2)$$

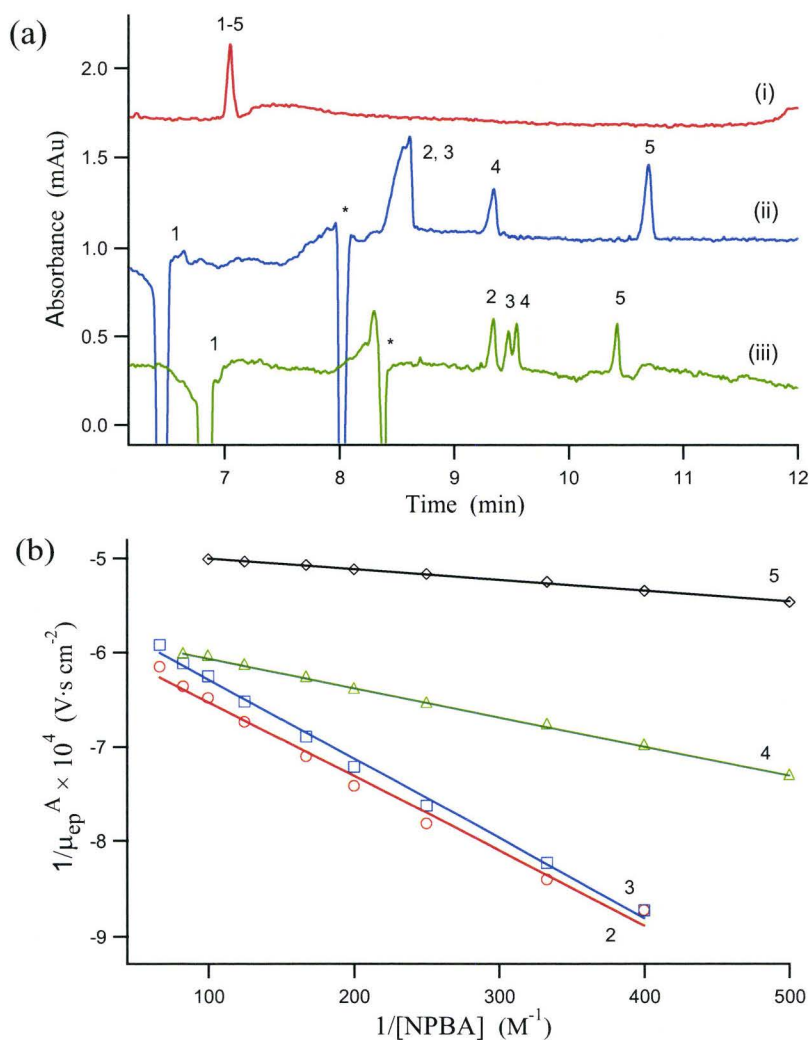


**Figure 2.5** (a) Electropherograms depicting the impact of increasing NPBA concentration in the background electrolyte for the separation and detection of polyols by DC-CE. Buffer conditions: 20 mM phosphate, pH 7.1 with (i) 0, (ii) 1, (iii) 3 and (iv) 12 mM NPBA. All other operating conditions as described in Figure 2.1. (b) Double-reciprocal binding isotherm plots used for determination of thermodynamic and electrokinetic parameters influencing NPBA-polyol separations by DC-CE based on eq (1), where open shapes represent average mobility data ( $n = 3$ ,  $CV < 1\%$ ) and solid lines represent line of best fit determined by linear regression. Peak numbering in plots correspond to 100  $\mu\text{M}$  of (1) resorcinol, (2) mannitol, (3) galactitol, (4) sorbitol and (5) catechol.



**Table 2.2** Thermodynamic and electrokinetic parameters influencing polyol separation with NPBA using 27 mM phosphate, pH 6.8 by DC-CE.

Analyte	$K_b^{\ddagger}$ ( $M^{-1}$ )	$\Delta H^{\circ  }$ ( $kJ\ mol^{-1}$ )	$T\Delta S^{\circ  }$ ( $kJ\ mol^{-1}$ )	$\mu_{ep,AC-}^{\ddagger} \times 10^{-4}$ ( $cm^2/Vs$ )
1. Mannitol	(497 ± 17)	-(10.4 ± 2.3)	(5.1 ± 2.2)	-(1.68 ± 0.02)
2. Galactitol	(453 ± 13)	-(10.5 ± 2.5)	(4.8 ± 2.4)	-(1.77 ± 0.02)
3. Sorbitol	(1255 ± 46)	-(19.4 ± 2.6)	-(1.6 ± 2.6)	-(1.72 ± 0.01)
4. Catechol	(2760 ± 290)	-(17.0 ± 2.8)	(2.8 ± 2.8)	-(2.05 ± 0.04)

<sup>†</sup> Parameters determined at 25°C, where the average mobility ( $n=3$ ) of free 3-NPBA was  $-(7.36 \pm 0.02) \times 10^{-5}$  <sup>||</sup> Thermodynamic parameters were derived from binding isotherms ( $n=3$ ) at five different temperatures ranging from 20-40°C

where,  $\mu_{ep}^A$  is the apparent mobility of polyol,  $K_b^*$  is the apparent binding constant and  $\mu_{ep,AC-}$  represent the mobility of the ternary NPBA-polyol-phosphate complex. It is apparent that the magnitude of binding affinity is inversely related to the slope of the plot, with catechol >> sorbitol >> mannitol > galactitol, which reflects the apparent migration order except for mannitol and galactitol.

The relative migration order of the latter two polyols can be explained in terms of the magnitude of  $\mu_{ep,AC-}$  for each NPBA-polyol complex, which is related to the reciprocal of the y-intercept. In general, maximum binding affinity was observed at pH 7.1, but it significantly decreased at lower (pH

6.4) and higher (pH 7.8) buffer pH conditions. **Table 2.2** summarizes the thermodynamic and electrokinetic parameters impacting polyol resolution by DC-CE under optimum conditions, which also includes catechol. Further studies were performed to systematically optimize buffer conditions to maximize polyol stereoisomer resolution, as well as absorbance response for micromolar detection of urinary polyols by DC-CE.

## 2.8 Central Composite Design for Separation Optimization.

Since newborn screening for galactosemia require methods that offer high efficiency resolution of elevated galactitol from other neutral polyol stereoisomers, a central composite design was performed to enhance polyol resolution by DC-CE based on three major experimental factors, namely buffer pH, phosphate concentration and capillary temperature. **Table 2.3** summarizes the variables, ranges and conditions used in the central composite experimental design for polyol resolution by DC-CE. A total of 19 experiments were performed over the experimental range while measuring two responses related to the resolution of mannitol-galactitol and galactitol-sorbitol. **Figure 2.6(a)** compares the magnitude of the coefficients for each variable (*i.e.*, single, 2-way, 3-way and quadratic) after multiple linear regression of data matrix, which clearly indicated that

**Table 2.3** Experimental variables, ranges and conditions selected in the central composite design<sup>†</sup> for optimization of polyol resolution by DC-CE.

Level	pH	[Phosphate] (mM)	Temperature (°C)
-1.7	6.4	3	16.5
-1	6.7	10	20
0	7.1	20	25
1	7.5	30	30
1.7	7.8	37	33.5

<sup>†</sup> Experimental design was performed as a single replicate for all conditions except for zero condition which was done (n=5) for a total of 19 experiments

buffer pH and phosphate concentration were the most significant factors impacting polyol resolution. **Figure 2.6(b)** depicts a correlation plot that demonstrates a good fit of the empirical model by comparison of measured and predicted polyol resolution throughout the experimental domain with normal error distribution. Two empirical equations based on a linear combination of the variable coefficients were then used to generate 3D surface response models for prediction of polyol resolution as depicted in **Figure 2.7(a) and (b)**. Surface response models provided clear visualization of optimal conditions to maximize the resolution of both pairs of polyol stereoisomers under a single experimental condition. Two different response curves were measured in this study, which represent the resolution between mannitol-galactitol (2-3) and galactitol-sorbitol (3-

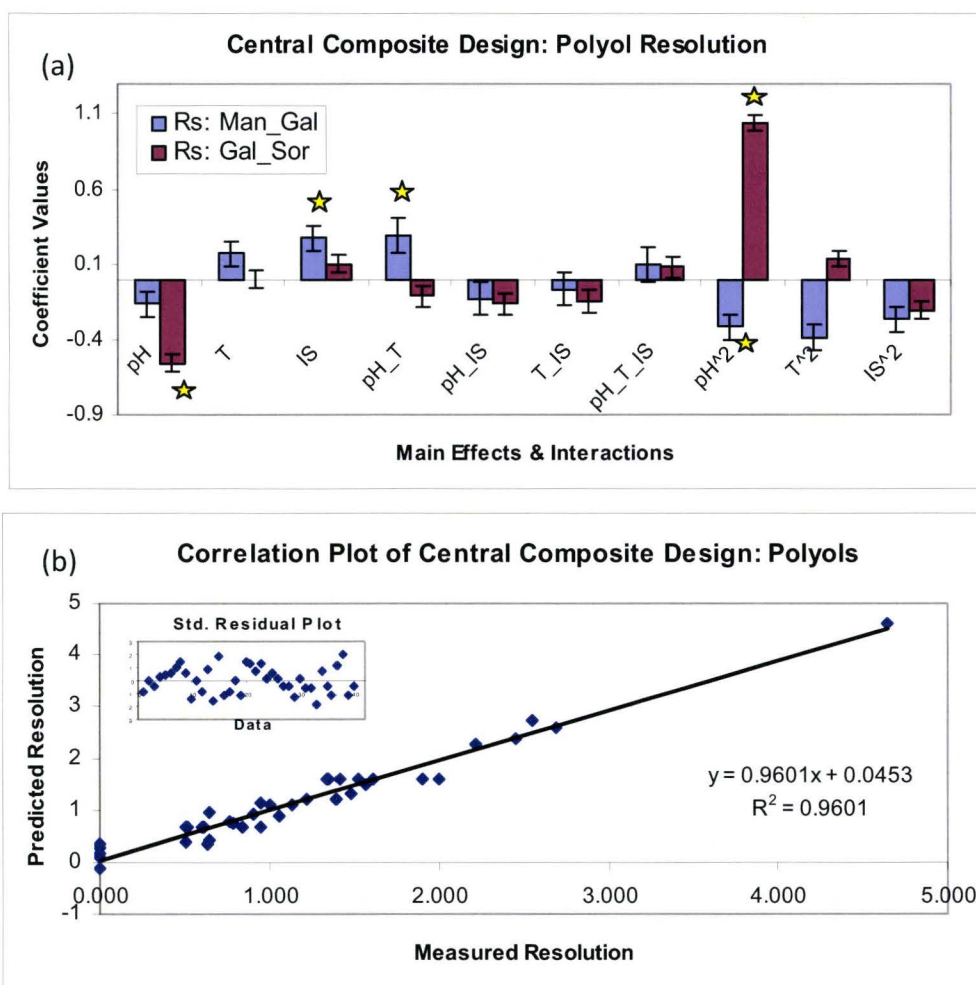


**Figure 2.6** (a) A summary of single, two-way, three-way and quadratic variables on resolution response for mannitol-galactitol and galactitol-sorbitol using a central composite design model, where stars highlight significant factors at 95% CL. Overall, buffer pH (pH) and phosphate concentration (IS) were the most significant experimental variables unlike column temperature (T). Empirical equations for polyol resolution based on the coefficient terms for the variables were used to construct 3D surface response models. (b) Correlation plot ( $n = 38$ ) of measured and predicted polyol resolution showing good linearity and normal error distribution reflected by the standardized residual plot shown as an inset.

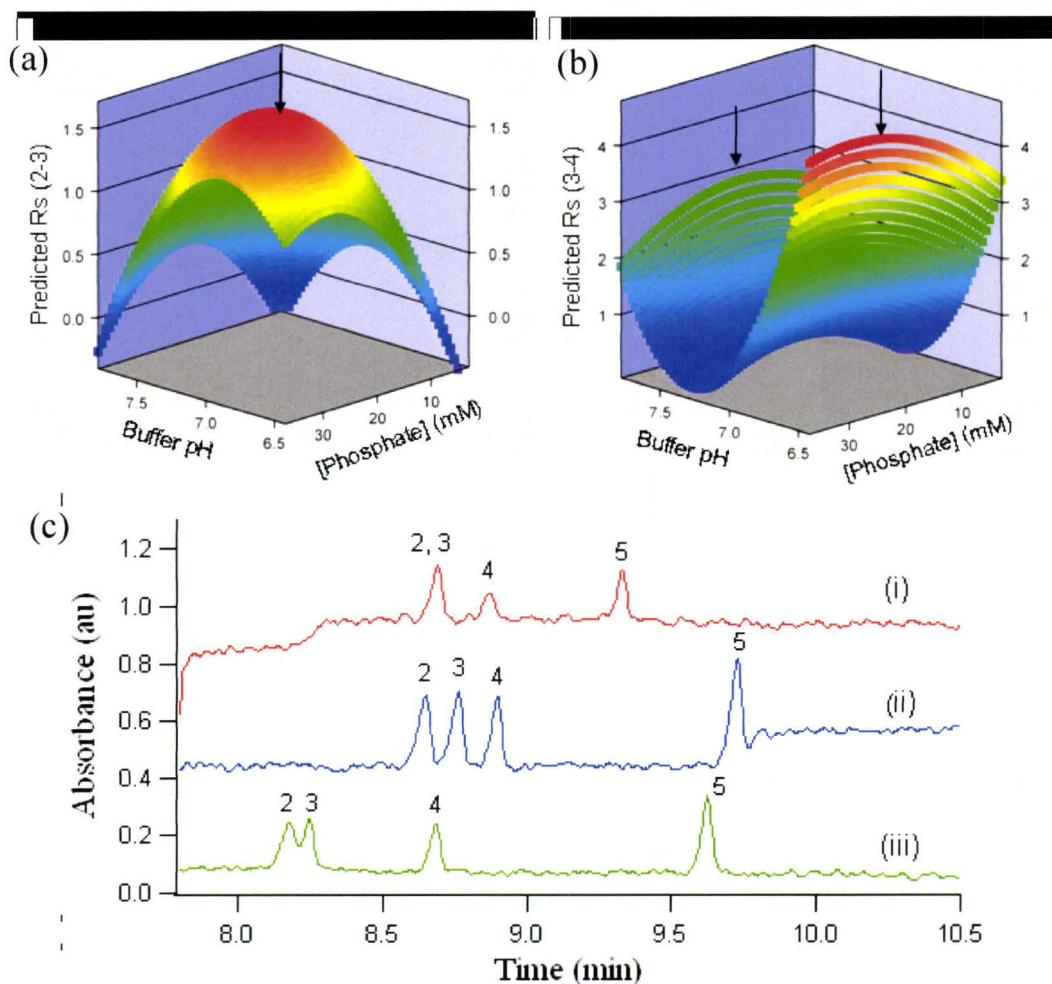


**Figure 2.7** Surface response models based on a central composite design for the optimization of polyol resolution by DC-CE, namely (a) mannitol-galactitol and (b) galactitol-sorbitol. Three distinct experimental conditions that maximize polyol resolution are indicated by an arrow. (c) Experimental electropherograms for validating optimum conditions predicted by surface response models, where (i) 17 mM phosphate, pH 7.8, (ii) 27 mM phosphate, pH 6.9 and (iii) 27 mM phosphate, pH 6.4.

4). It is apparent that optimal resolution for each pair of polyol isomer occurs under distinct conditions. For instance, a single maximum resolution condition is predicted for mannitol-galactitol (2-3) at 27 mM

phosphate, pH 6.9, whereas two maxima conditions are indicated for galactitol-sorbitol (3-4) at 17 mM phosphate, pH 7.8 and 27 mM phosphate, pH 6.4. Thus, buffer pH was the most significant variable impacting polyol resolution, which does not necessarily relate to operating under pH conditions above the  $pK_a$  of the boronic acid. **Figure 2.7(c)** depicts an overlay of experimental electropherograms based on the three optimal conditions predicted by the surface response models. The greatest resolution for galactitol-sorbitol (3-4) was achieved at 27 mM phosphate, pH 6.4 as shown in **Figure 2.7(c)iii**, however this condition resulted in only partial resolution of mannitol- galactitol (2-3). Similarly, **Figure 2.7(b)i** highlights excellent resolution concentration generates less Joule heating at the higher buffer pH with reduced band broadening, but also decreases the polyol signal response. In contrast, **Figure 2.7(c)ii** demonstrates that separation using 27 mM phosphate, pH 6.9 achieves baseline resolution of both mannitol-galactitol (2-3) and galactitol-sorbitol (3-4), although the latter resolution was decreased relative to **Figure 2.7(b)iii**. Overall, the optimal electrolyte condition to ensure maximum resolution of both pairs of polyols was determined to be 27 mM phosphate, pH 6.8 at 25°C, which was used for the remaining part of this study.

## 2.9 Role of Phosphate and NPBA in the Direct UV Detection of Polyols.

Although the importance of the composition of electrolyte solution on the apparent binding behavior of polyols to boronic acids has been noted by several groups, to the best of our knowledge, this is the first report that highlights the benefit of specific electrolytes on the spectral properties of boronic acid probes. **Figure 2.8(a)** depicts a series of electropherograms that highlight the direct dependence of polyol signal with increasing phosphate concentration ranging from 3, 7 and 27 mM. It is important to emphasize that all polyols (100  $\mu$ M) were also improved polyol resolution due to the slower electroosmotic flow (EOF) and longer residence time for separation. **Figure 2.8(b)** summarizes the phosphate-dependence on the average peak area response for polyols and catechol. Despite being intrinsically responsive at UV 280 nm, the molar absorptivity of catechol in fact was enhanced about eight-fold at higher phosphate concentration. However, the most dramatic effect was with the polyols, where a linear increase in absorbance response was measured from 3-20 mM which peaked near 27 mM phosphate, whereas subsequent higher concentrations did not significantly change its absorbance.

The use of other common buffer electrolytes, including carbonate and MES, did not generate a similar UV response for polyols compared to

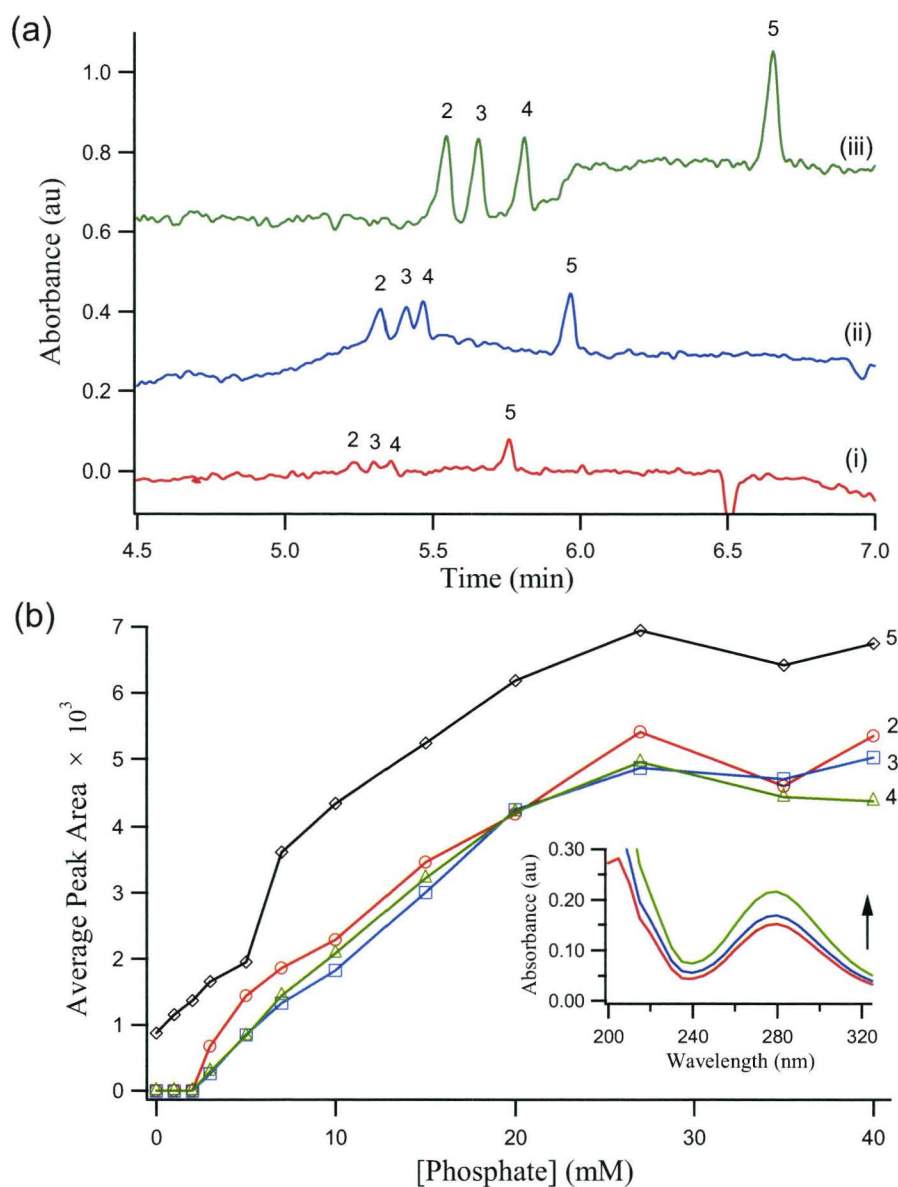


**Figure 2.8** (a) Electropherograms highlighting the impact of phosphate concentration of the absorbance response for 100  $\mu\text{M}$  polyols at 280 nm using (i) 3, (ii) 7 and (iii) 27 mM phosphate with 15 mM NPBA, pH 6.8. (b) Overall trend depicting dramatic increase in the average peak area ( $n = 3$ ) for UV-transparent polyols as well as UV-responsive catechol at higher phosphate concentration in the background electrolyte. The inset of (b) shows an overlay of UV spectra for NPBA that confirms the enhancement in molar absorptivity at 280 nm with higher phosphate concentration (3, 7 and 27 mM).



phosphate (data not shown). Since phosphate is itself UV-transparent at 280 nm, phosphate clearly does not function merely as a passive electrolyte for pH control, but also selectively interacts with NPBA to enhance NPBA spectral response upon polyol complexation. These observations are consistent with previous studies regarding the role of phosphate in modifying the apparent acidity of boronic acids, as well as their complexation behavior. The inset of **Figure 2.8(b)** demonstrates the effect of increasing phosphate concentration on the spectral properties of the NPBA-sorbitol complex, which resulted in an enhancement in its molar absorptivity at 280 nm ( $\Delta\epsilon$ ) of  $3,200 \text{ M}^{-1}\text{cm}^{-1}$  from 3 to 27 mM phosphate. Further evidence of direct phosphate association with NPBA was also confirmed by NMR experiments, which qualitatively demonstrated that the electronic environment of both phosphorus and boron undergo significant changes as a result of boronic acid complexation with phosphate and sorbitol. This process was vital for inducing the spectral changes in NPBA required for direct absorbance detection of polyols by DC-CE, which is consistent with the formation of the tetrahedral NPBA-sorbitol-phosphate ternary complex depicted in **Figure 2.1** of this chapter.

## 2.10 NMR Studies of Ternary Complex Formation.

Further evidence of direct phosphate association with NPBA was

also provided by  $^{31}\text{P}$  and  $^{11}\text{B}$ -NMR experiments as shown in **Figure 2.9**. Overall, significant changes in the chemical shift of both  $^{31}\text{P}$  and  $^{11}\text{B}$  resonances were observed for phosphate and NPBA solutions relative to their free states. For instance, there was a relative upfield shift ( $\Delta\delta$ ) in the  $^{31}\text{P}$  resonance for phosphate (27 mM, pH 6.8) of -0.49 and -0.65 ppm with the addition of 15 mM NPBA and 15 mM NPBA with 3 mM sorbitol, respectively. In contrast, the addition of 3 mM sorbitol alone (without NPBA) did not produce any significant change in phosphate chemical shift (data not shown). Similarly, there was a major relative upfield chemical shift ( $\Delta\delta$ ) in the  $^{11}\text{B}$  resonance for NPBA in de-ionized water (no phosphate) of -8.84 and -7.32 ppm with the addition of 27 mM phosphate and 27 mM phosphate with 3 mM sorbitol, pH 6.8, respectively. In addition, the latter condition generated a new high upfield resonance ( $\Delta\delta$ ) at -22.24 ppm, which is characteristic of the tetrahedral NPBA-sorbitol-phosphate ternary boronate ester complex as depicted in **Figure 2.1** of this chapter. These NMR experiments qualitatively confirm that the electronic environment of both phosphorus and boron undergo significant changes as a result of boronic acid complexation with phosphate and sorbitol as ligands/Lewis bases, which was vital for inducing the apparent UV spectral changes in NPBA required for direct absorbance detection of polyols by DC-CE.

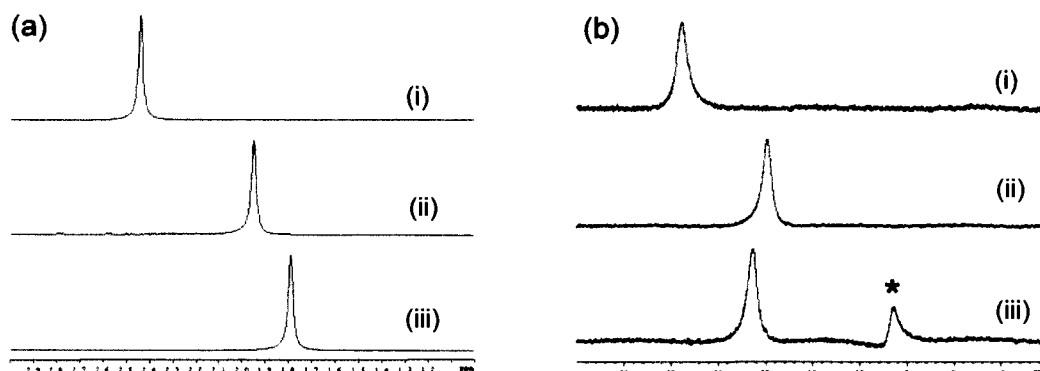


**Figure 2.9** (a)  $^{31}\text{P}$ -NMR spectra showing distinct upfield chemical shift changes for phosphate at pH 6.8 as a function of electrolyte composition, (i) 27 mM phosphate, (ii) 27 mM phosphate, 15 mM NPBA and (iii) 27 mM phosphate, 15 mM NPBA, 3 mM sorbitol. (b)  $^{11}\text{B}$ -NMR spectra depicting upfield chemical shift changes for NPBA at pH 6.8 as a function of electrolyte composition, (i) 15 mM NPBA in de-ionized water, (ii) 27 mM phosphate, 15 mM NPBA and (iii) 27 mM phosphate, 15 mM NPBA, 3 mM sorbitol. The extra peak noted by \* in (b)(iii) represents the ternary NPBA-sorbitol-phosphate boronate ester complex as depicted in Figure 2.1 of this chapter.

## 2.11 Method Validation

Validation studies for DC-CE were performed using 15 mM NPBA in 27 mM phosphate, pH 6.8 with 1.5 mM  $\text{MgCl}_2$  as the optimum separation condition, which provided the maximum resolution of all three polyol stereoisomers. The addition of 1.5 mM  $\text{Mg}^{2+}$  in the background electrolyte (data not shown) effectively reduced the EOF while not contributing significantly to Joule heating or altering the selectivity of polyol separation. This provided polyols longer residence time in the capillary for separation with resolution exceeding 3.0 that also included the analysis of galactonate and gluconate that are clinically relevant secondary

**Table 2.4** Method validation for single-step analysis of polyols by DC-CE under optimum separation conditions using 27 mM phosphate, 15 mM NPBA, 1.5 mM MgCl<sub>2</sub>, pH 6.8.

Validation Parameters	Mannitol	Galactitol	Sorbitol
<i>1. Reproducibility (n = 10)</i>			
Relative Migration Time (CV, %)	0.3	0.3	0.2
Relative Peak Area (CV, %)	3.4	7.4	4.8
<i>2. Calibration Curve<sup>†</sup> (n = 6)</i>			
Linearity ( $R^2$ )	0.9951	0.9973	0.9933
<i>3. Detection Limit (S/N ≈ 3)</i>			
LOD ( $\mu\text{M}$ )	20	20	20
<i>4. Accuracy<sup>‡</sup> (n = 10)</i>			
Recovery in Urine (%)	92	86	104

<sup>†</sup> Calibration curve range from 50-420  $\mu\text{M}$  performed in triplicate at six different concentrations using relative peak areas to the internal standard catechol. <sup>‡</sup> Recovery studies performed by spiking 100  $\mu\text{M}$  polyols in a healthy urine sample using ten replicates.

metabolites present in urine. **Table 2.4** summarizes the overall validation parameters in terms of linearity, LOD, accuracy and precision.

The detection limit ( $S/N \approx 3$ ) was determined to be about 20 $\mu\text{M}$ , which provided sufficient sensitivity for diagnosis of galactosemia and related sugar metabolic disorders associated with elevated polyol concentrations ( $\approx 1$  mM). The average recovery ( $n = 10$ ) of a 100  $\mu\text{M}$  spiked urine sample containing the three neutral polyol stereoisomers was determined to be about 94 %. Method reproducibility ( $n = 10$ ) for urine analysis by DC-CE was also assessed in terms of relative peak area and

relative migration time using catechol as the internal standard, which provided good precision as reflected by an average CV of 5.2 and 0.3%, respectively. The major advantage of DC-CE is its high selectivity which permits excellent resolution of polyol stereoisomers without interferences in complex biological samples, while offering low cost, simplicity and convenience since it does not require labor-intensive or time-consuming off-line sample pretreatment steps prior to analysis.

## **CHAPTER III**

### **3. High-throughput Screening of Holoprotein Conformational Stability by Dynamic Ligand Exchange- Affinity Capillary Electrophoresis**

*\*This chapter of thesis is derived from the published manuscript:*

G. Seguí-Lines, J. M. A. Gavina , J. C. D'Amaral and P. Britz-McKibbin \*  
*Analyst*, **2007**, 132: 741-744 (Communication). DOI: 10.1039/b705469f

*Reproduced by permission of ©The Royal Society of Chemistry*

### 3.1 Abstract

Dynamic ligand exchange-affinity capillary electrophoresis (DLE-ACE) is introduced as a convenient platform for assessing the conformational stability and relative affinity of a holoprotein to different ligands without off-line sample pretreatment, since ligand exchange and protein unfolding processes are integrated in-capillary during electromigration.

### 3.2 Introduction

Ligand binding plays a crucial role in regulating protein conformation, activity and function. In order to assess the impact of a ligand on protein stability, conventional techniques based on optical spectroscopy, microcalorimetry and NMR compare the resistance to chemical or thermal denaturation of the ligand-free apoprotein relative to the holoprotein complex. However, off-line sample preparation of apoprotein and/or ligand-exchanged holoprotein by partial unfolding with equilibrium dialysis is time-consuming and labor-intensive.<sup>1</sup> Moreover, the *apo* state is often unstable and susceptible to proteolysis, whereas the preparation of a ligand-exchanged holoprotein can generate misfolding. Thus, new strategies are needed for the rapid preparation of different protein states when using small amounts of sample. This is the case for cyclic AMP

(cAMP)-dependent protein kinase (cAPK), which is a ubiquitous holoprotein involved in cell signaling.<sup>1</sup> The inactive apoprotein tetramer consists of a regulatory dimer subunit and two catalytic subunits. cAMP binding to the regulatory subunits induces an allosteric conformational change, resulting in dissociation of catalytic subunits with kinase activity.<sup>1</sup> Herein, we demonstrate that DLE-ACE offers a single-step format for comparative *apo/holo* thermodynamic studies of a regulatory type I alpha (RI $\alpha$ ) cAPK associated with different cyclic nucleotides (cNTs) as a model system. Since sample preparation is integrated during analysis, DLE-ACE is conducive for high-throughput screening of drug candidates for cyclic nucleotide binding proteins, such as guanine exchange factors and cGMP-dependent protein kinases.<sup>2</sup> Unlike recent high-throughput screening strategies based on MS,<sup>3</sup> DLE-ACE offers a unique format for *in-situ* generation and characterization of different protein states in solution without off-line apoprotein preparation and complicated sample handling procedures.

ACE is a high resolution microseparation technique that is increasingly being applied as a physical tool to quantify biomolecular interactions.<sup>4</sup> However, ACE is often not suitable for studying high affinity protein interactions with small ligands that induce negligible changes in



protein mobility. Selective fluorescent labeling of the ligand (e.g. cAMP) can be performed to overcome this challenge; however, this can modify its intrinsic binding to a receptor, as well as imparting additional time and cost constraints on the assay.<sup>5</sup> Alternatively, ACE experiments can be performed *via* assessment of the relative stability of the *apo/holo* protein states upon unfolding.<sup>3b,c</sup> This strategy not only enables determination of apparent ligand dissociation constant ( $K_d$ ), but also provides holoprotein conformational stability ( $\Delta G_U^0$ ) and cooperativity ( $m$ ) parameters. Although CE has been used to study protein unfolding, it is still an unrecognized technique for characterizing holoprotein systems.<sup>6</sup> Recently, our group demonstrated reversible *holo*-R1 $\alpha$ -cAMP dissociation by CE, which permitted *in-situ* generation of the labile *apo* state *via* electrophoretic ligand-stripping.<sup>6b</sup> In this study, DLE-ACE with laser-induced native fluorescence (LINF) detection is introduced as a convenient yet rapid format for comparative thermodynamic studies of R1 $\alpha$  involving different cNT analogues.

### 3.3 Theory

**Figure 3.1** illustrates the principle of DLE-ACE where the apoprotein (R1 $\alpha$ ) is first generated upon voltage application from the initial holoprotein (R1 $\alpha$ -cAMP) that is injected as a short sample plug with excess cAMP.

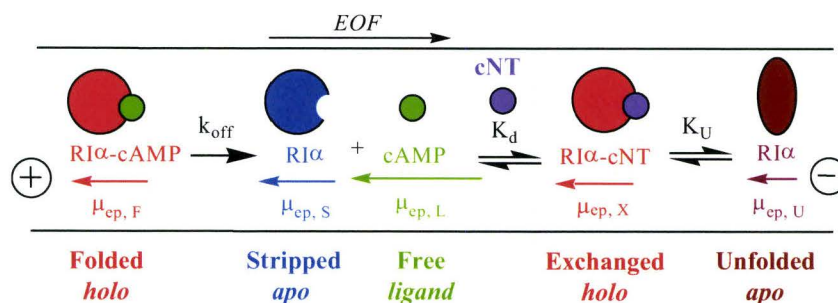


**Figure 3.1** Three-step process depicting dynamic cAMP-stripping, cNT exchange and *holo*-RI $\alpha$ -cNT unfolding by DLE-ACE, where arrow vectors represent the electrophoretic mobilities ( $\mu_{ep}$ ) of different protein/ligand states.

cAMP-stripping is mediated electrokinetically without chemical denaturant since the negative mobility of the small ligand is greater than the bulky ligand-stripped protein (*i.e.*  $\mu_{ep,L} > \mu_{ep,S}$ ). This process is also favorable due to the fast dissociation rate constant ( $k_{off} \approx 60s^{-1}$ ) for RI $\alpha^{1d}$  when performing separations in buffer devoid of ligand. Owing to the reversibility of complex formation, ligand exchange can be realized during *apo*-RI $\alpha$  electromigration by the addition of excess cNT to the background electrolyte since the original ligand (*i.e.* cAMP) is irreversibly separated from the protein. When the same process is performed in the presence of urea, the exchanged *holo*-RI $\alpha$ -cNT (X) undergoes denaturation into the unfolded *apo*-RI $\alpha$  (U) state, where  $\mu_{ep,U} < \mu_{ep,X}$ . In this case, ligand-stripping and exchange must precede protein unfolding<sup>‡</sup> (*i.e.*  $k_{off} > k_U$ ) to ensure adequate equilibration prior to detection, otherwise changes in

buffer conditions will not alter the apparent thermodynamic parameters. Assuming a reversible two-state unfolding process for R1 $\alpha$ ,<sup>1</sup> the apparent free energy ( $\Delta G_U$ ) for unfolding can then be measured by changes in the viscosity-corrected apparent mobility (*i.e.*  $v\mu_{ep}^A$ ) as a function of urea concentration.<sup>6b</sup> Alternatively, the fraction of unfolded protein ( $F_U$ ) can be determined by **equation 3.1**, which allows for direct comparison of protein denaturation curves:

$$F_U = \frac{v\mu_{ep}^A - \mu_{ep,F}}{\mu_{ep,U} - \mu_{ep,F}} \quad (3.1)$$

$F_U$  data determined by DLE-ACE then allow determination of  $\Delta G_U^0$  and  $m$  by **equation 3.2** using the linear extrapolation method, where  $c$  is the urea concentration:

$$\Delta G_U = -RT \frac{F_U}{(1 - F_U)} = \Delta G_U^0 + mc \quad (3.2)$$

Comparison of  $\Delta G_U^0$  of *apolholo* protein states associated with different cNT analogues also permits estimation of the apparent dissociation energy<sup>§</sup> ( $\Delta G_d^0$ ) of protein–ligand interactions,<sup>1e</sup>

$$\Delta G_d^0 \approx \Delta \Delta G_U^0 - RT \ln[L] \quad (3.3)$$

where,  $\Delta\Delta G_U^0$  is the difference in free energy of the *apo/holo* states ( $\Delta G_{U,holo}^0 - \Delta G_{U,apo}^0$ ) and  $[L]$  is the free ligand concentration. The major advantage of DLE-ACE is that it permits direct injection of low amounts of stable holoprotein (<100 fmol per injection) without sample pretreatment, extrinsic fluorescent/ radiolabels and sample pre-incubation. The latter feature was feasible due to fast unfolding kinetics of the protein relative to the separation timescale.

### 3.4 Results and Discussion

R1 $\alpha$  is a weakly acidic ( $pI \approx 5.3$ )<sup>6b</sup> truncated protein construct (14.1 kDa) having two Trp residues at positions 188 and 222 within a single cAMP binding domain that serves as a good model for cyclic nucleotide binding.<sup>7</sup> **Figure 3.2(a)** depicts an overlay of a series of electropherograms showing distinct mobility changes for *apo* and three different *holo*-R1 $\alpha$ -cNT states in 6 M urea by DLE- ACE. All separations were performed using a short-end injection at the electrolyte outlet, which enabled rapid analyses of under 5 min. This faster separation format was also important for achieving more reliable mobility measurements of the labile *apo*-R1 $\alpha$  state relative to our preliminary report,<sup>6b</sup> which was hampered by excessive

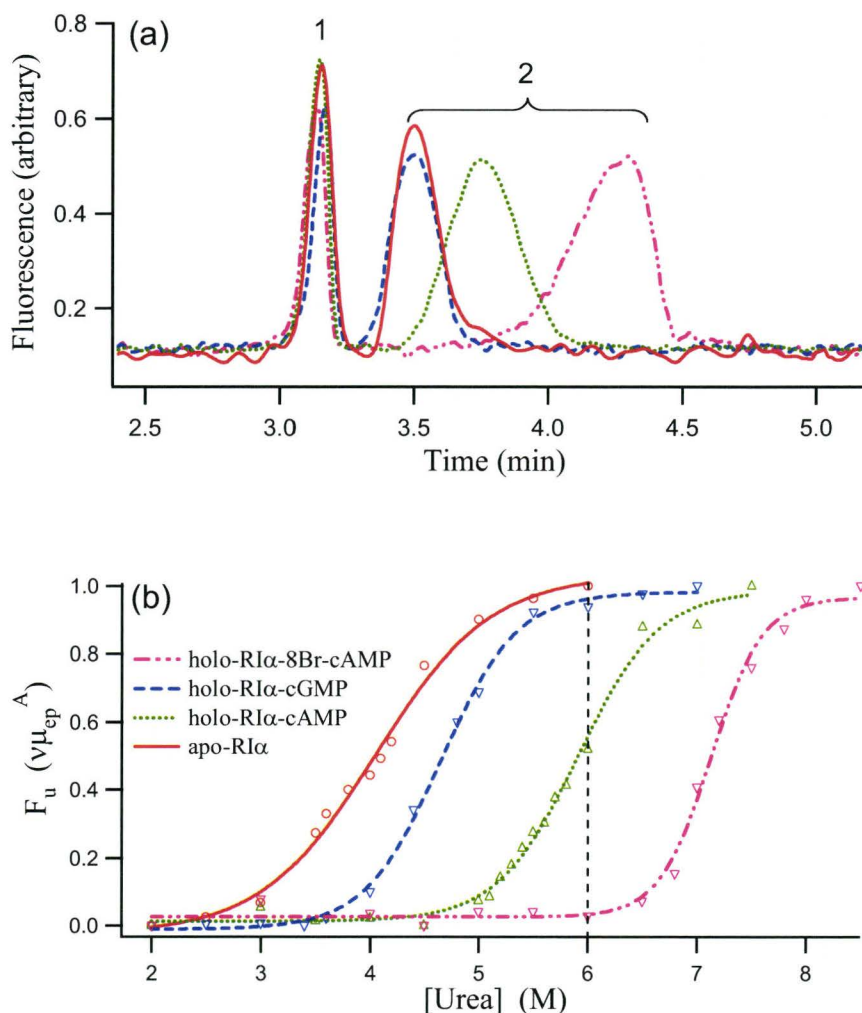


**Figure 3.2** Impact of ligand on conformational stability of R1 $\alpha$ , where (a) depicts overlay electropherograms for different *apo/holo*-protein states in 6 M urea, and (b) compares *apo/holo*-protein unfolding curves as a function of cNT by DLE-ACE using LINF detection at 337 nm with 266 nm excitation.<sup>||</sup> Peaks correspond to (1) neutral EOF marker, melatonin and (2) R1 $\alpha$ . Data are based on triplicate measurements with the coefficient of variation (CV) under 2%.

peak broadening at low urea concentrations. This feature was critical for ensuring accurate relative holoprotein stability and affinity measurements.

In fact, thermodynamic parameters measured for *apo/ho* states of R1 $\alpha$ -cAMP in this study<sup>1f</sup> were consistent with independent experiments performed by fluorescence spectroscopy on the wild-type R1 $\alpha$  that contains two cAMP binding domains.<sup>1c</sup> It is apparent that each protein state (2) has a distinct stability reflective of its characteristic  $\mu_{ep}^A$  relative to the neutral EOF marker (1) due to association with the cNT during electromigration. For instance, *apo*-R1 $\alpha$  and *ho*lo-R1 $\alpha$ -cGMP co-migrate as the unfolded protein state in 6 M urea, whereas *ho*lo-R1 $\alpha$ -cAMP and *ho*lo-R1 $\alpha$ -8BrcAMP migrate as partially unfolded and fully folded states, respectively. Thus, these studies qualitatively demonstrate that ligand binding has a differential impact on R1 $\alpha$  stability that is associated with the magnitude of its affinity for each cNT analogue.

**Figure 3.2(b)** compares the R1 $\alpha$  unfolding curves as a function of excess cNT, representing four distinct protein states generated by DLE-ACE, namely (i) *apo*-R1 $\alpha$ , (ii) *ho*lo-R1 $\alpha$ -cAMP, (iii) *ho*lo-R1 $\alpha$ -cGMP, and (iv) *ho*lo-R1 $\alpha$ -8BrcAMP. It is clear that cAMP association results in enhanced stability of *apo*-R1 $\alpha$  by about 6 kcal mol<sup>-1</sup> with a 2 M increase in the urea mid-point concentration ( $C_M$ ). In contrast, **Figure 3.2(b)** demonstrates that excess cGMP confers a less significant increase in stabilization relative to *apo*-R1 $\alpha$  of only 3 kcal mol<sup>-1</sup>. Indeed, there is great interest in better understanding the cross-talk between cAMP and cGMP in the signal

**Table 3.1** Comparison of thermodynamic parameters for conformational stability and relative binding affinity of *holo*-R1 $\alpha$ -cNT by DLE-ACE.

<i>holo</i> -R1 $\alpha$ (Ligand)	$\Delta C_M^b$ (M)	$\Delta m^b$ (kcal/mol·M)	$\Delta\Delta G_U^0$ <sup>b</sup> (kcal/mol)	$K_{d,cAMP} / K_{d,cNT}$
cAMP	1.9	-(0.7 $\pm$ 0.1)	(5.9 $\pm$ 0.5)	1
cGMP	0.7	-(0.6 $\pm$ 0.1)	(3.1 $\pm$ 0.5)	(0.083 $\pm$ 0.007)
8-BrcAMP	3.1	-(0.7 $\pm$ 0.1)	(8.1 $\pm$ 0.9)	(42 $\pm$ 5)

<sup>a</sup> Parameters derived from linear regression of R1 $\alpha$  unfolding curves, where error represents  $\pm 1\sigma$

<sup>b</sup> Differences in  $C_M$ ,  $m$  and  $\Delta G_U^0$  of *holo*-R1 $\alpha$  to *apo*-R1 $\alpha$  states

transduction pathway within cells since cAMP has been reported to activate cGMP-dependent protein kinases.<sup>8a</sup> However, binding of the membrane-permeable cAMP analogue, 8-BrcAMP, suggests a major enhancement in R1 $\alpha$  conformational stability of 8 kcal mol<sup>-1</sup> relative to *apo*-R1 $\alpha$ , which is consistent with its higher affinity and full agonist activity.<sup>8b</sup>  $\Delta\Delta G_U^0$  values in **Table 3.1** can also be used to estimate dissociation constants using **Equation 3.3**. The relative affinity (*i.e.*,  $K_{d,cAMP} / K_{d,cNT}$ ) of 8-BrcAMP and cGMP to R1 $\alpha$  was determined by DLE-ACE to be about 40-fold greater and 120-fold weaker than cAMP, respectively, which offers a more convenient format relative to traditional competitive radiolabel assays.<sup>8b</sup> In addition, it was determined that the unfolding cooperativity ( $m$ ) for *holo*-R1 $\alpha$ -cNT was similar for each cNT, but enhanced by about -0.7 kcal mol<sup>-1</sup> M<sup>-1</sup> relative to *apo*-R1 $\alpha$ . This feature is

useful for selecting ligand candidates in terms of their binding affinity and ordering effect on global protein conformation for subsequent structural or *in-vitro* activity studies.

### 3.5 Conclusions

It is anticipated that DLE-ACE will play an increasing role as a promising platform for assessing the conformational stability of holoproteins with cyclic nucleotide binding domains. The advent of multiplexed capillary array instruments provides a high-throughput environment for screening ligand libraries for activity against protein targets. For instance, about 4500 ligands per day could be screened using a single commercial 96 capillary array electrophoresis instrument with a microtitre sample plate. This assumes a 10 min total run time per sample that includes capillary conditioning/sample handling, while using three urea denaturant conditions<sup>3b</sup> to estimate relative ligand affinity. Although the SUPREX method<sup>3b</sup> has been reported to be able to screen greater than 10,000 ligands per day, this does not take into account the time required for apoprotein preparation, which is often the major bottleneck in HTS of labile ligand-free receptor targets. To the best of our knowledge, no other technique offers similar advantages for seamlessly integrating sample preparation for the rapid characterization of holoprotein stability



and the relative binding affinity to different ligands. Future work is directed at expanding the applicability of DLE-ACE for characterizing other protein–ligand systems. In conclusion, DLE-ACE offers a versatile format for comparative thermodynamic studies that is complementary with protein conformational mapping by NMR.<sup>7a,b</sup>

### 3.6 References

- 1 (a) D. A. Johnson, P. Akamine, E. Radzio-Andzelm, M. Madhusudan and S. S. Taylor, *Chem. Rev.*, 2001, **101**, 2243 External Links; (b) D. A. Leon, J. M. Canaves and S. S. Taylor, *Biochemistry*, 2000, **39**, 5662 External Links; (c) J. M. Canaves, D. A. Leon and S. S. Taylor, *Biochemistry*, 2000, **39**, 15022 External Links; (d) M. Zorn, K. E. Fladmark, D. Ogreid, B. Jastorff, S. O. Doskeland and W. R. G. Dostmann, *FEBS Lett.*, 1995, **362**, 291 External Links; (e) C. N. Pace and T. McGrath, *J. Biol. Chem.*, 1980, **255**, 3862 External Links.
- 2 J. L. Bos, *Trends Biochem. Sci.*, 2006, **31**, 680 External Links; I. McPhee, L. C. D. Gibson, J. Kewney, C. Darroch, P. A. Stevens, D. Spinks, A. Cooreman and S. J. MacKenzie, *Biochem. Soc. Trans.*, 2005, **33**, 1330 External Links; W. R. Dostmann, W. Tegge, R. Frank, C. K. Nickl, M. S. Taylor and J. E. Brayden, *Pharmacol. Ther.*, 2002, **93**, 203 External Links.
- 3 (a) S. M. Clark and L. Konermann, *Anal. Chem.*, 2004, **76**, 7077 External Links; (b) K. D. Powell and M. C. Fitzgerald, *J. Comb. Chem.*, 2004, **6**, 262 External Links; (c) K. D. Powell, S. Ghaemmaghami, M. Z. Wang, L. Ma, T. G. Oas and M. C. Fitzgerald, *J. Am. Chem. Soc.*, 2002, **124**, 10256 External Links.
- 4 M. Berezovski, A. Drabovich, S. M. Krylova, M. Musheev, V. Okhonin, A. Petrov and S. N. Krylov, *J. Am. Chem. Soc.*, 2005, **127**, 3165 External Links; E. E. Jameson, J. M. Cunliffe, R. R. Neubig, R. K. Sunahara and R. T. Kennedy,

- Anal. Chem.*, 2003, **75**, 4297 External Links; N. H. H. Heegaard, *Electrophoresis*, 2003, **24**, 3879 External Links; X. C. Le, Q. H. Wan and M. T. Lam, *Electrophoresis*, 2002, **23**, 903 External Links; R. C. Tim, R. A. Kautz and B. L. Karger, *Electrophoresis*, 2000, **21**, 220 External Links; L. Z. Avila, Y. H. Chu, E. C. Blossey and G. M. Whitesides, *J. Med. Chem.*, 1993, **36**, 126 External Links.
- 5 (a) C. Mucignat-Caretta and A. Caretta, *Biochim. Biophys. Acta*, 1997, **1357**, 81 External Links; (b) A. Caretta, D. Cevolani, G. Luppino, M. Matelli and R. Tirindelli, *Eur. J. Neurosci.*, 1991, **3**, 669 External Links.
- 6 (a) J. M. A. Gavina and P. Britz-McKibbin, *Curr. Anal. Chem.*, 2007, **3**, 17 External Links; (b) J. M. A. Gavina, R. Das and P. Britz-McKibbin, *Electrophoresis*, 2006, **27**, 4196 External Links; (c) D. Rochu, C. Cléry-Barraud, F. Renault, A. Chevalier, C. Bon and P. Masson, *Electrophoresis*, 2006, **27**, 442 External Links; (d) P. G. Righetti and B. Verzola, *Electrophoresis*, 2001, **22**, 2359 External Links.
- 7 (a) R. Das and G. Melacini, *J. Biol. Chem.*, 2007, **282**, 581 External Links; (b) R. Das, M. Abu-Abed and G. Melacini, *J. Am. Chem. Soc.*, 2006, **128**, 8406 External Links; (c) L. J. Huang and S. S. Taylor, *J. Biol. Chem.*, 1998, **273**, 26739 External Links.
- 8 (a) D. A. Pelligrino and Q. Wang, *Prog. Neurobiol.*, 1998, **56**, 1 External Links; (b) W. R. G. Dostmann, S. S. Taylor, H. G. Genieser, B. Jastorff, S. O. Doskeland and D. OGREID, *J. Biol. Chem.*, 1990, **265**, 10484 External Links.

### 3.7 Footnotes

‡ **Figure 3.1** is viable only if the rate of cAMP-stripping and cNT exchange is faster than protein unfolding (*i.e.*,  $k_{\text{off}}(\text{cAMP}) > k_{\text{on}}(\text{cNT}) > k_{\text{U}}$ ). This feature ensures that irreversible separation of cAMP with cNT association occurs prior to urea-induced unfolding of *holo*-R1 $\alpha$ -cNT in the background

electrolyte. All protein samples were prepared in MES buffer in excess cAMP (0.2 mM) without urea in order to ensure long-term stability of the holoprotein. Thus, no sample pre-incubation in urea was required for equilibration prior to DLE-ACE, since R1 $\alpha$  was observed to undergo fast unfolding kinetics relative to the separation timescale (e.g., 5 min). This property was verified by performing time-dependent unfolding studies of R1 $\alpha$  (i.e., 0–1.5 hrs) pre-incubated in 4 and 6 M urea prior to CE without observing any significant changes in apparent protein mobility. The major advantage of DLE-ACE is that ligand-stripping/exchange processes can be readily controlled through simple modification of the electrolyte conditions.

§ This relationship assumes a reversible protein unfolding process where ligand interaction occurs only with the folded native protein state when using excess ligand that is equivalent to its equilibrium concentration (i.e. 200  $\mu$ M). Refolding experiments were performed by unfolding *holo*-R1 $\alpha$ -cAMP in 7 M urea off-line prior to DLE-ACE analyses in a buffer with excess cAMP but devoid of urea. No apparent misfolded or conformational intermediates were evident in these studies due to correlation in measured refolded protein  $v\mu_{ep}^A$  with the folded state. This confirmed the reversibility of *holo*-R1 $\alpha$ -cAMP unfolding and the validity of the measured

thermodynamic parameters. All CE data were transformed into standard fraction of protein unfolding ( $F_U$ ) plots in order to normalize the mobility values of the different protein states that facilitated comparative analyses.

<sup>¶</sup> In this study,  $\Delta G^\circ_U$  for *apo*-R1 $\alpha$  and *holo*-R1 $\alpha$ -cAMP states were determined to be  $(3.7 \pm 0.2)$  and  $(9.6 \pm 0.5)$  kcal mol<sup>-1</sup>, whereas  $m$  values were  $-(0.9 \pm 0.1)$  and  $-(1.6 \pm 0.1)$  kcal mol<sup>-1</sup> M<sup>-1</sup>, respectively. Improved correlation with literature values<sup>1c</sup> was achieved compared to our earlier study,<sup>6b</sup> notably for the labile *apo*-R1 $\alpha$  by using a faster separation format to minimize protein band dispersion.

<sup>¶¶</sup> All separations were performed on a P/ACE MDQ CE system equipped with dual-channel laser-induced fluorescence interface (Beckman-Coulter Inc., Fullerton, CA, USA). Uncoated fused-silica capillaries with 75  $\mu$ m i.d., 360  $\mu$ m o.d. and 30 cm length (Polymicro Technologies, Phoenix, USA) were used for the analyses. Each day the capillary was first conditioned by high pressure rinsing for 5 min with 0.1 M NaOH, 5 min in deionized water and 10 min in the background electrolyte. Subsequent unfolding studies were then preceded by a 2 min rinse with 0.1 M NaOH and a 3 min rinse with the background electrolyte prior to each separation. Owing to the high concentration of urea used throughout the experiments, the electrodes and capillary interface in the CE instrument were cleaned regularly each

day to prevent significant salt residue accumulation and sample contamination. Separations were thermostated at 25 °C using a reversed polarity voltage of –8 kV since sample injections were performed at the electrolyte outlet. This short-end injection format enabled rapid analyses under 5 min with an effective capillary length of 10 cm to the detector. Although the capillary ends were not thermostated, this was not a significant issue since relative thermodynamic parameters were measured. In addition, separations were operated within the linear region of an Ohm plot to reduce electrolyte-induced heating effects. Native fluorescence excitation at 266 nm (average power output ca. 2 mW) was performed using a diode-pumped solid-state Q-switched Nd-YAG laser (CryLaS GmbH, Berlin, Germany) coupled to the CE instrument with a UV multimode fiber patchcord (Oz Optics, Carp, Ontario), whereas detection was performed at 337 nm using a narrow bandpass (FWHM  $\pm$  10 nm) emission filter (Andover Corporation, Salem, USA). Hydrodynamic injection of samples was performed at the capillary outlet using a low pressure (0.5 psi or 3.5 kPa) for 5 s. All separations were performed in 100 mM MES, pH 6.5 (adjusted by 0.1 M NaOH) buffer with excess cyclic nucleotide (200  $\mu$ M cNT) and/or urea. Separation buffers containing cNT and urea were prepared prior to use from stock solutions in 100 mM MES pH 6.5. A stock solution of 10 mM melatonin was also prepared in water

and added to the sample prior to analysis. DLE-ACE studies required less than 100 fmol of  $R1\alpha$  (e.g. 40  $\mu\text{M}$  in 30  $\mu\text{L}$ ) sample containing excess cAMP (280  $\mu\text{M}$ ). The concentration sensitivity can be further enhanced by using broad bandpass detection filters with appropriate digital noise filtering.

## **CHAPTER IV**

### **4. Future applications and directions**

#### 4. Future applications and directions

The work presented in this thesis is a contribution to a novel approach for high-quality screening using CE as an integrative platform for separating and detecting stereoisomers and various protein states while providing kinetic and thermodynamic parameters for characterizing reversible covalent boronic acid-polyol and non-covalent protein-small molecule interactions. Several unique methodologies have been developed to efficiently integrate labour-intensive sample pre-treatment steps that are applicable to both proteins and metabolites during chemical analysis in CE, such as in-capillary *apo/olo*-protein generation with dynamic protein unfolding and on-line dynamic complexation of neutral and UV transparent hexitol stereoisomers. Integration of these steps offers an integrated analytical strategy which reduces complicated sample handling and total analysis times often associated with the processing complex biological samples prior to analysis. Together, these projects represent significant advances in the application of CE useful for improved methods in clinical diagnosis (*e.g.*, galactosemia) and drug development (*e.g.*, synthetic inhibitors). The strategies developed in this thesis are particularly relevant towards improving high-quality drug screening by offering a label-free screening method for allosteric ligands to



regulatory/receptor protein targets (e.g.,  $R\alpha$ ). For instance, DLE-ACE introduced a novel strategy for thermodynamic assessment of allosteric proteins based on multiple parameters associated with *holoprotein* conformational stability, unfolding cooperativity and ligand binding affinity. This approach allows for the determination of high affinity binding interactions over a wide dynamic range ( $K_d \approx$  nM-mM) without chemical labelling of protein or ligand, which also has promising applications for differentiating orthosteric and allosteric binding events which is not feasible by conventional primary screening methods, such as competitive radiolabel or fluorescence assays.

In addition, our work demonstrated that CE provides a convenient method for stereoselective resolution of polyols that was achieved based on their differential electromigration behavior with NPBA in phosphate buffer. Direct photometric detection of  $\mu$ M levels of hexitol stereoisomers in urine samples was also realized via *in-situ* generation of a UV-active anionic ternary boronate ester complex, providing very promising features for inhibitors and newborn screening of galactosemia. Similar to most in-born errors of metabolism (IEMs), early detection of such disorders is crucial for preventing irreversible delays in newborn development, which often can be treated by dietary adjustments (e.g., galactose/lactose-free products). Recent methods developed for galactitol analysis based on GC-

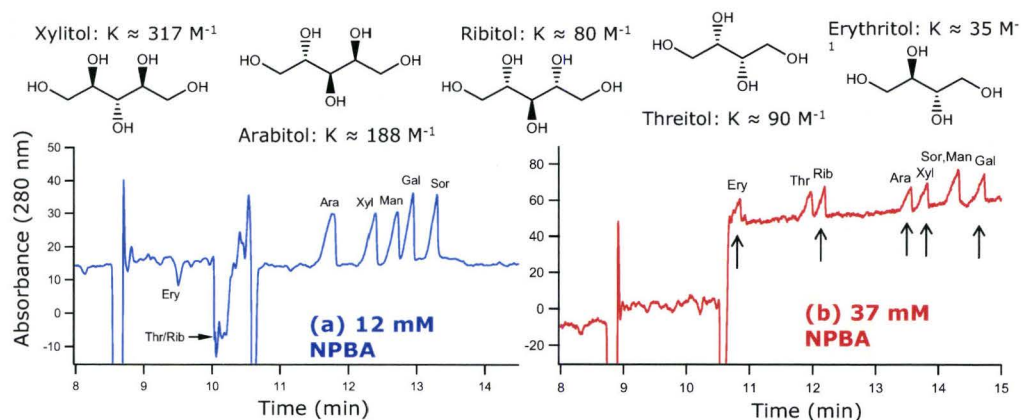


**Figure 4.1** Recent work carried out by our group to extend the applicability of boronic acid-hexitol interactions for resolution of C<sub>4</sub>, C<sub>5</sub> and C<sub>6</sub>-polyols using two different concentrations of NPBA.

MS<sup>1</sup> and LC-MS<sup>2</sup> are time-consuming and often do not provide sufficient resolution of hexitol stereoisomers. In contrast, our method offers a simple and direct strategy for hexitol analysis without off-line sample pretreatment, which can be translated into high-throughput screening based on commercially available 96 capillary array electrophoresis systems. Future work will be carried out to extend the applicability of DC-CE for single-step analysis of polyol stereoisomers in biological samples using other derivatives of arylboronic acids (e.g., pyridineboronic acids), as well as extending the method to resolve and detect micromolar concentrations of C<sub>4</sub>, C<sub>5</sub>, and C<sub>6</sub>- polyols of varying chain length, such as erythritol and threitol (C<sub>4</sub> polyols or tetrityls) and ribitol, arabitol and xylitol (C<sub>5</sub> polyols or pentityls) as shown in **Figure 4.1**. Recently, two new rare

inborn errors of polyol metabolism were identified, namely of transaldolase (TALDO) and ribose-5-phosphate isomerase (RPI)<sup>3</sup> deficiencies, which can be diagnosed by elevated urinary concentrations of erythritol, arabitol and ribitol, whereas xylitol is only mildly elevated relative to a normal control population.<sup>92</sup> **Figure 4.1** depicts the preliminary work that is being carried out in our research group regarding the extension of DC-CE for analysis of several polyols relevant to the diagnosis of TALDO and RPI, which highlights that binding affinity decreases significantly with short-chain polyols (e.g., C<sub>4</sub>), but it is also dependent on the specific configuration of hydroxyl moieties. Future work will focus on characterizing different analogues of arylboronic acids that possess higher affinity with polyols relative to NPBA in order to improve concentration sensitivity/detectability of our method, which is limited by the high concentrations of NPBA needed to be used in the BGE to achieve sufficient resolution of polyol stereoisomers.

Another extension of this thesis realized in our laboratory is related to our protein unfolding project. Recently, a label-free strategy has been published by Gavina et al<sup>4</sup> for determination of the thermodynamic parameters associated with holoprotein unfolding and allosteric ligand binding for the exchange protein directly activated by cAMP (EPAC) protein. There is growing interest in the development of ligands that

selectively target EPAC due to its altered expression in several chronic disorders, such as Alzheimer's disease.<sup>4</sup> **Figure 4.2** depicts the chemical structures of six different cNT analogues, as well as an overlay of protein unfolding curves derived from DLE-ACE experiments, which highlights the significant impact of ligand binding on holoprotein conformational stability. Multivariate analysis of thermodynamic parameters associated with holoprotein unfolding and ligand binding was demonstrated for the classification/selection of cyclic nucleotide analogues that function as allosteric modulators of regulatory proteins such as EPAC when using principal component analysis (PCA). To date, DLE-CE is limited in regards the time regime of protein unfolding dynamics. When the studied protein unfolds slowly relative to the electrophoretic separation scale (slow time regime), the protein requires off-line pre-incubation, for achieving equilibrium prior to the separation. In this case, as well as when the protein unfolds with intermediates or reversible refolds, initial characterization of the protein-ligand system and optimization of the CE experimental conditions will need to be determined notably for large multimeric proteins or membrane-bound protein systems. Thus, when applying DLE-ACE to new classes of proteins, a kinetic analysis of the rate of protein unfolding in urea as a function of time will need to be adequately

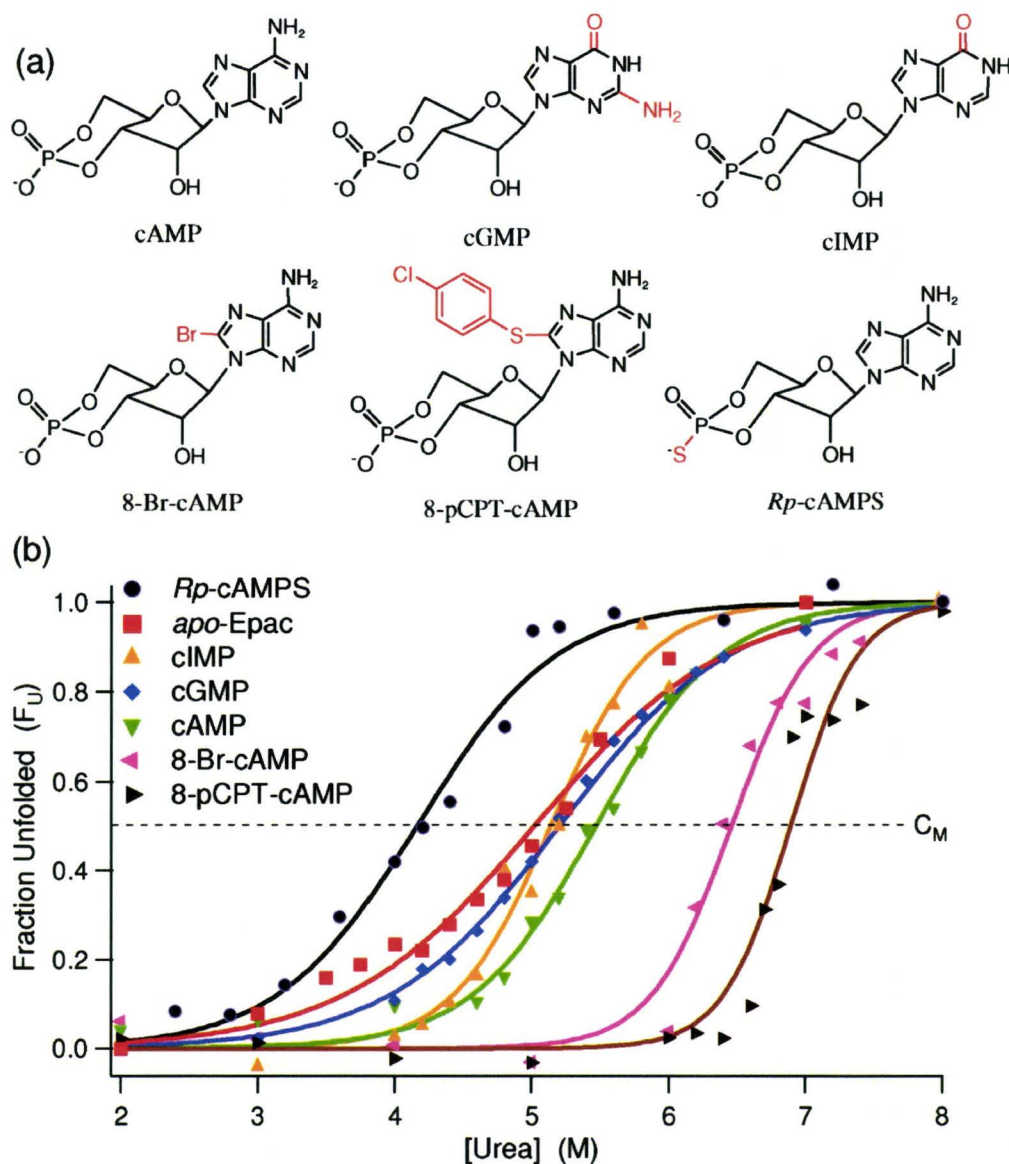


**Figure 4.2** Impact of cNT binding on the conformational stability of EPAC upon urea denaturation by DLE-ACE, where (a) shows two-dimensional chemical structures of different cNT analogues and (b) compares apo/holo protein unfolding curves based on the average viscosity-corrected apparent mobility of protein,  $v\mu_{ep}^A$  (symbols;  $n = 3$ , CV < 5%) assuming an ideal two-state model, where  $C_M$  represents the midpoint for urea denaturation ( $F_u = 0.5$ ). Reprinted with permission from Gavina J.M.A., Mazhab-Jafari M.T., Melacini G., Britz-McKibbin P., *Biochem. J.* 48 (2009) 2, 223 -225.<sup>5</sup> Copyright (2008) with permission from American Chemical Society.

assessed. Some other limitations exist, such as the possibility of protein adsorption to the capillary surface during separation when working with uncoated capillaries at  $\text{pH} > 3$ . Covalent and dynamic non-covalent coatings<sup>6,7</sup> can be then used to modify the capillary wall to be neutral and hydrophilic provided that they do not alter ligand binding to the protein.

The methods presented in this thesis demonstrate the versatility of CE as a unified platform for the characterization of biomolecular interactions involving proteins and/or metabolites that can contribute to improvements to high-quality drug screening and clinical diagnosis of in-born errors of metabolism. Improved sample throughput, along with low-cost analyses and with access to multiple thermodynamic/kinetic parameters will allow for better selection of putative drug candidates, as well as a deeper understanding of the fundamental processes operative in separation science.

## 4.1 References

---

- 1 Lee J., Chung B.C., *J. Chromatogr. B* **831** (2006) 126-131.
- 2 Wamelink M., Smith D., Jakobs C., *J. Inherit. Metab. Dis.* **28** (2005) 951-963.
- 3 Wamelink M. M. C., Struys E. A., Jakobs C., *J. Inherit. Metab. Dis.* **31** (2008) 703-717.
- 4 McPhee I., Gibson L. C. D., Kewney J., Darroch C., Stevens P. A., Spinks D., Cooreman A., and MacKenzie S., *J. Biochem. Soc. Trans.* **33** (2005) 1330-1332.
- 5 Gavina J.M.A., Mazhab-Jafari M.T., Melacini G., Britz-McKibbin P., *Biochemistry* **48** (2009) 223-225
- 6 Horvath J., Dolnik V., *Electrophoresis* **22** (2001) 664-675
- 7 Righetti P.G., Gelfi C., Verzola B., Castelletti L., *Electrophoresis* **22** (2001) 603-611

## **Chapter V**

### **5. Appendix**



## **5.1 Covalent Boronate Ester Complexation**

### **5.1.1 Introduction**

The formation of a boronic ester complex with a neutral polyol is a very strong yet selective reversible covalent binding interaction in an aqueous environment that can be readily used for the construction of molecular receptors. Consequently, boronic acids have been used as a common recognition motif in the construction of sensors for saccharides,<sup>1</sup> as nucleotide and carbohydrate transporters,<sup>2</sup> and as affinity ligands for the separation of carbohydrates and glycoproteins.<sup>3</sup> Appropriately designed boronic acid compounds also have shown potential as antibody mimics targeted to cell-surface carbohydrates.<sup>4</sup> Critical to furthering these efforts is an understanding of the various factors that have an impact on the relative stability of boronate esters. Boronic acid/polyol binding affinities can be determined through a recently developed competitive fluorescent assay that is not limited by the requirement for a fluorescent boronic acid, which allows to for the determination of the binding constants for a series of polyols with phenylboronic acid analogues.<sup>5</sup>

### 5.1.2 $pK_a$ and binding constant determination

A phenylboronic acid (PBA) is an aryl substituted boric acid containing a carbon to boron bond belonging to the class of organoboranes. PBA's act as Lewis acids and possess a unique feature in that they are capable of forming reversible covalent complexes with sugars or other molecules possessing 1,2- vicinal diols.<sup>6</sup>

The stability of the boronate ester is pH- and solvent-dependent,<sup>6</sup> but the factors that govern these processes are not well understood. Using a three component competitive assay containing the fluorescent compound Alizarin Red S (ARS), phenylboronic acid (PBA), and a diol-containing compound, the stability of a series of boronate esters was studied and their binding constant were determined.<sup>6</sup> By using a fluorescent reporter as the measuring tool, ester stabilities were monitored under a variety of conditions that included changes in pH, buffer and solvent. This was in direct contrast to the commonly used pH-depression methods,<sup>7</sup> where the increase in acidity seen when a diol is titrated into a solution of boronic acid was measured. The method required the boronic acid to be used as the buffer, and measured association over a 'floating pH'. The three-component approach allowed examining the details of the equilibrium formation while pH and buffer can be varied, and clarified the relationships between association constants. The apparent  $pK_a$  of each boronic acid

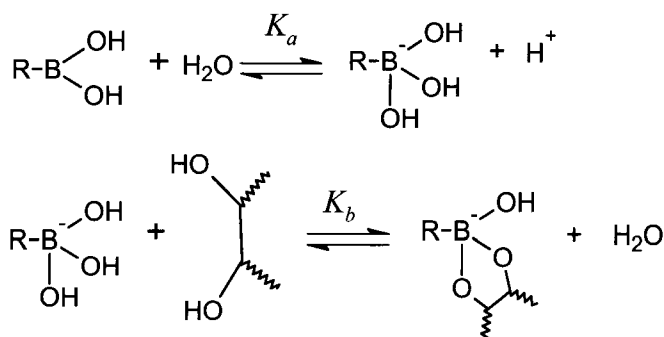


**Figure 5.1** The thermodynamic relationships between boronic acid and its diol ester.

was determined by observing the UV absorption changes that occur upon the hybridization change from the acidic trigonal form to the conjugate basic tetrahedral structure (**Figure 1.5**). When at a pH higher than its  $pK_a$ , PBA will assume its anionic, tetrahedral form through the binding of a hydroxyl group from a water molecule (**Figure 1.5**). In this anionic structure, the formation of a boronic ester with vicinal diols is favoured, endowing the complex with a negative charge. If the vicinal diol is a sugar alcohol, the sugar alcohol-phenylboronic acid complex now has intrinsic charge and a detectable phenyl moiety, both of which are amenable traits for separation in CE, as it will be demonstrated in **Chapter 2** of this thesis.

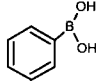
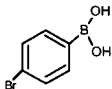
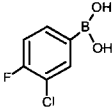
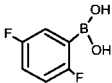
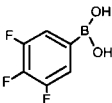
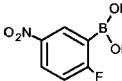
### 5.1.3 Effect of substituents on $pK_a$ of boronic acids

To determine the effect of different boronic acid acidities upon binding, a series of arylboronic acids with different substituents and two *N*-

alkylated pyridinium boronic acids were examined.<sup>5</sup> At the extremes of this series were the electron rich 2-methoxyphenylboronic acid with the highest  $pK_a$  at 9.0, and the cationic *N*-benzylpyridinium boronic acid with the lowest  $pK_a$  at 4.2. With the  $pK_a$  values of these boronic acids spanning about 5  $pK_a$  units, its effect on the binding constants were examined over a wide range. As expected, electron-withdrawing groups decreased the  $pK_a$  and electron-donating groups increased their  $pK_a$  as depicted in **Table 1**. However, it does seem that the effect of electron donating groups is marginal compared with the electron withdrawing groups. For example, the  $pK_a$  of 2-methoxyphenyl boronic acid is only 0.2  $pK_a$  units higher than that of PBA (8.8), while the  $pK_a$  of 3-nitrophenyl boronic acid (NPBA) is 1.7  $pK_a$  units lower than that of PBA. The availability of this  $pK_a$  data serves as a baseline reference for the future design of arylboronic acid sensors with optimal affinity and specificity at physiological pH. Note that the specific electron-withdrawal group on NPBA makes this PBA an ideal boronic acid derivative for the complexation and separation of polyols at physiological pH, as described in **Chapter 2** of this thesis.

In an effort to examine the relationship among  $pK_a$ , pH, and  $K_b$  in a broader sense, the binding constants were determined for 6 substituted phenylboronic acids with glucose, fructose, and catechol at different pH

**Table 4.1  $pK_a$  and  $K_b$  values of a series of substituted PBA compounds<sup>5</sup>**

Arylboronic acid	Structure	$pK_a$	$K_b$ (glucose-PBA) @ pH 7.5 ( $M^{-1}$ )	$K_b$ (fructose-PBA) @ pH 7.5 ( $M^{-1}$ )
Phenylboronic acid		8.8	4.6	210
4-Bromophenylboronic acid		8.8	20	495
3-Chloro-4-fluorophenylboronic acid		7.8	26	1003
2,5-Difluorophenylboronic acid		7.0	47	2136
3,4,5-Trifluorophenylboronic acid		6.8	41	2523
2-Fluoro-5-nitrophenylboronic acid		6.0	47	2062

values, and the results with fructose are summarized in **Table 1**. First, the ranking of the binding constants among different boronic acids with a given diol at physiological pH does not always follow the trend of the boronic acid  $pK_a$ . For example, although 2,5-difluorophenylboronic acid has a higher apparent  $pK_a$  (7.6) than 3,4,5-trifluorophenylboronic acid (6.8), it also has a higher binding constant with glucose at pH 7.5, which

goes against the conventional thinking. On the other hand, the ranking of the binding constants for these two boronic acids with fructose is reversed compared to binding with glucose. It is also interesting to note that the binding constants of 2,5-difluorophenylboronic acid and 3,4,5-trifluorophenylboronic acid with fructose at pH 7.5 are higher than that of 2-fluoro-5-nitrophenylboronic acid even though the latter has the lowest  $pK_a$  among all six boronic acids tested. Consequently, the results indicate that, as expected, electron-withdrawing groups can significantly lower the  $pK_a$  of boronic acids, while boronic acids with lower  $pK_a$  values do not always show greater binding affinities.

#### 5.1.4 Sensors for Saccharides

There is considerable interest in developing saccharides sensors due to their broad utility in wide-ranging applications. Saccharide sensors are needed anywhere from the food and cosmetic industries to medicinal and academic arenas. The most common interactions between phenylboronic acids and saccharides are with *cis*-1,2- or 1,3-diols of saccharides to form five or six-membered rings, respectively. These covalent bonds are rapidly and reversibly formed between a diol and boronic acid ( $sp^3$ -hybridized) in aqueous solution. Formation of an  $sp^3$ -hybridized boronic acid is possible in a basic pH region (boronate anion) or by incorporation of a neighboring tertiary amine (B-N bond) at neutral

pH. The B-N bond has been successfully used in the development of saccharide sensors. The interaction of the neighboring amine with the boronic acid is strengthened on saccharide binding. The strength of this boronic acid–tertiary amine interaction can be used to signal the binding event.

For applicability in biological and medicinal arenas, it is crucial that these sensors operate in aqueous media at physiological pH. Difficulties associated with developing saccharide sensors result from the fact that saccharides contain one kind of recognition unit (the hydroxyl functional group) and that they lack a spectroscopic handle, such as a chromophore or fluorophore, whose modulation can be harnessed in a sensing scheme. Although myriad biosensors have been reported, many lack the durability necessary for widespread usage in real-world settings. By contrast, chemosensors are being increasingly used in real-world settings, offering the advantage of not only greater durability than their biological counterparts but also flexibility in their design: signaling units affording various sorts of readouts (*e.g.*, circular dichroism, colorimetric, fluorescent, and electrochemical) are readily incorporated, and their design can be synthetically optimized and modified.

Two main approaches have been employed in the design of synthetic receptors, starting points for the chemosensing of saccharides.

The first approach involves the use of supramolecular hosts tailored with complementary hydrogen-bonding binding sites with saccharides primarily in nonaqueous media.<sup>8</sup> This approach has mainly been used in academic arenas in the development of biomimetic systems for studying protein–carbohydrate hydrogen bonding interactions. It has found limited utility in real-world settings, hampered by the difficulty in synthesizing these receptors and effecting molecular recognition in aqueous media.

The boronic acid moiety is featured in the second approach, either appended to elaborate scaffolds or used in simple constructs.<sup>9</sup> Reversible covalent cyclic ester formation of these moieties with diols of saccharides is the basis of this recognition motif. In contrast to the first approach, recognition of saccharides is effective in aqueous media under basic pH conditions, and with additional design elements, at physiological pH. These systems, however, routinely lack a high degree of selectivity for a particular saccharide, with the exception of fructose, due to the lack of selectivity of the boronic acid in terms of binding affinity, and are often difficult to synthesize and purify.

Pattern-based discrimination of analytes derived from array sensing schemes holds great promise in meeting the challenges faced by new saccharide sensors. This research area, coined as “differential sensing”, has emerged as a powerful tool for detecting chemically diverse analytes,



discriminating subtly different compounds within each class of analytes, and detecting mixtures thereof.<sup>10</sup> Thus, moderately selective boronic acid based receptors such as those described previously are well-suited for this approach, but the process of identifying a series of suitable receptors with varying degrees of selectivity for targeted saccharides is complex and time-consuming. Irrespective of this, some studies of pattern-based discrimination of saccharides have been recently achieved. Severin and co-workers have used an indicator displacement assay consisting of a rhodium complex and galloxyanine at different pH values for the discrimination of amino sugars and aminoglycosides.<sup>11</sup> Chang *et al* have reported the colorimetric discrimination of 23 saccharides (mainly monosaccharides and disaccharides) at 100mM concentration using boric and boronic acids with pH indicators.<sup>12</sup> Also, Singaram also recently used boronic acid bipyridinium salts to differentiate among twelve saccharides at 2 mM concentration by using a fluorescent sensor array at physiological pH values.<sup>13</sup> Alternatively, **Chapter 2** of this thesis introduced a strategy that uses electrophoretic separations as a format to expand the selectivity of arylboronic acid molecular recognition to polyol stereoisomers.

### 5.1.5 Polyols: Significance and Metabolism

Hexitols are a specific subset of a group of compounds known as sugar alcohols or polyols. Sugar alcohols or polyols are a hydrogenated form of carbohydrate whose carbonyl group has been reduced to a primary hydroxyl group. Polyols possess low digestibility, and therefore are common replacements for sucrose in food products. They are not metabolized by oral bacteria so they do not contribute to tooth decay and since they are incompletely absorbed into the blood stream from the intestine they result in a smaller change in blood glucose than regular sugars.<sup>14</sup> All these properties make polyols popular food ingredients. However, in the aldose-reductase (AR) deficiencies under hyperglycemia conditions, polyol pathways accelerate the accumulation of polyols which leads to early tissue damage.<sup>15</sup> For example, excess sorbitol (Sor) in the cells of the eyes and nerves has been linked to diabetic retinopathy and neuropathy in diabetes mellitus.<sup>16,17</sup> Similarly, galactitol (Gal) represents a clinically useful biomarker that is excreted at elevated concentrations in the urine and plasma of patients affected with inborn errors of sugar metabolism.

The resolution between Man, Sor and Gal would prove to be difficult as they are neutral stereoisomers which do not intrinsically possess strong

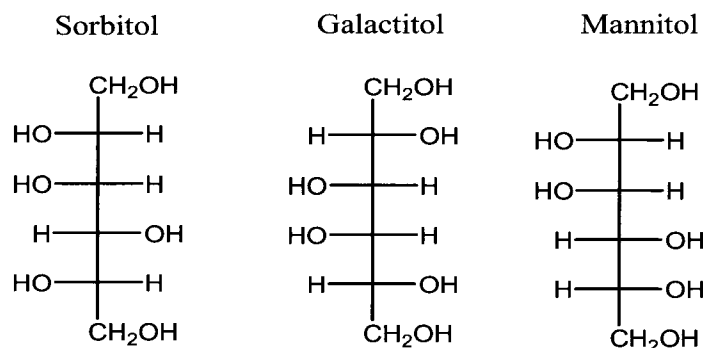


**Figure 5.2** Chemical structures of neutral stereoisomers of hexitols which do not intrinsically possess strong chromophores required for photometric detection.

chromophores for photometric detection (**Figure 1.7**).

Researchers have reported various methods to separate and detect this family of compounds, such as enzymatic assay<sup>18</sup>, HPLC with pulsed amperometric detection<sup>19</sup> and GC/MS.<sup>20</sup> Unfortunately, most of these methods are time-consuming and require extensive sample pretreatment and digestion procedures. As described in **Chapter 2** of this thesis, DC-CE will outline a single step analyte strategy that uses NPBA as an electrokinetic probe to enhance the selectivity and resolution of polyols, based on their differential electromigration behavior in phosphate buffer. Our strategy allows for direct photometric detection of  $\mu\text{M}$  levels of polyols isomers in urine samples via *in-situ* generation of a UV-active anionic ternary boronate ester complex.

## 5.2 Protein Unfolding and cNT Interactions

### 5.2.1 cAMP-dependent Protein Kinase: Structure and biological role

Many cellular signaling pathways in eukaryotes involve protein kinases, which phosphorylate Ser, Thr, and Tyr residues in a variety of target proteins.<sup>21</sup> Deregulation of kinase activity has been related to a wide range of diseases. For that reason, searching for potent inhibitors that are selective against the more than 500 potential human kinase targets is currently an active area of drug discovery.<sup>22</sup>

The cAMP-dependent protein kinase A (cAPK) is one of the best-studied members of the Ser/Thr protein kinase family<sup>23</sup>. cAPK is known to be involved in the regulation of a large number of cellular processes including metabolism, contractile activity, growth, apoptosis, and ion flux.<sup>21</sup> Mutations in protein kinase A (PKA) can lead to diseases such as Carney complex and Lupus. The catalytic (C) subunits of PKA are responsible for catalyzing the phospho-transfer reaction, whereas the regulatory (R) subunits serve both to confer cAMP dependence and to localize the holoenzyme to discrete subcellular locations via interactions with A-kinase anchoring proteins (AKAP's).<sup>21</sup> At low cAMP concentrations, PKA is maintained as an inactive tetrameric holoenzyme complex ( $R_2C_2$ ) consisting of a homodimeric  $R_2$  subunit and two C subunits. When intracellular concentrations of cAMP increase in response to specific

cellular stimuli, four cAMP molecules bind to each  $R_2$  subunit. This event causes a release of inhibition of C by R, allowing the C subunits to phosphorylate their target proteins. In addition to the regulatory subunits, specificity is also achieved by the scaffold proteins, the AKAP's, which target PKA through the regulatory subunits to different sites within the cell and in close proximity to specific substrates. All of these proteins contribute to the PKA signaling networks that permeate every mammalian cell. Each also contributes in novel ways to the dynamic features of this network.

The activity of the catalytic (C) subunit is regulated by a set of four different regulatory (R) subunit isoforms of PKA, types  $I\alpha$ ,  $I\beta$ ,  $II\alpha$ , and  $II\beta$ , which differ with respect to their R subunits ( $RI\alpha$ ,  $RI\beta$ ,  $RII\alpha$ , and  $RII\beta$ , respectively). Although each regulatory subunit has a conserved organization of subdomains with a dimerization/docking (D/D) domain at the amino terminus and two tandem cAMP binding domains at the carboxyl terminus, the R subunits play distinct roles and are not functionally redundant. It was determined by genetic studies in mice that the isoforms have different biological roles. For instance, mice lacking the  $RI\alpha$  gene died *in-utero*<sup>24</sup>, whereas mice lacking the  $RII\beta$  gene were viable, lean, and resistant to diet-induced obesity<sup>25</sup>. These differences are reflected also in the biochemistry of the two subunits. RI is not

phosphorylated and binds only to the ATP bound form of PKA. RII subunits are autophosphorylated and do not require ATP to bind. In RI subunits, the A domain binds cAMP with high affinity only when cAMP is bound to the B domain.<sup>26</sup>

### 5.2.2 Principles of Protein Unfolding

Proteins can be unfolded by increasing temperature or by adding chaotropic denaturant agents (*e.g.*, urea, guanidinium chloride) in order to disrupt protein non-covalent intermolecular interactions. Changes in protein conformations during unfolding can be probed in solution by several different spectroscopic formats that include circular dichroism, fluorescence and NMR. In general, each technique offers complementary qualitative information regarding protein unfolding dynamics ranging from long-range changes in peptide backbone structure to atomic resolution of specific amino acid residues. A non-spectroscopic technique that has also been widely used for assessing protein unfolding is differential scanning calorimetry.<sup>27, 28</sup> However, it is evident that no single method has found exclusive use for protein unfolding studies due to the limitations in the required sensitivity, selectivity and applicability to different types of protein systems. Thus, techniques that can be applied to a wider variety of samples, such as low amounts of recombinant protein, unfractionated

protein mixtures and multimeric holoprotein complexes, are desirable for future research.<sup>29</sup>

Rush *et al.*<sup>30</sup> introduced CE as a new method for examining protein conformational stability in 1991 that offered several unique advantages over traditional platforms, such as classical slab gel electrophoresis. Since then, over 70 different CE studies have been reported for protein unfolding with major contributions made by the groups of Righetti<sup>31</sup> and Rochu<sup>32</sup>. However, it still remains a rather unrecognized technique for characterizing protein conformational stability in the wider biochemical community. CE provides an automated electrophoretic format using small amounts of sample and reagents. Moreover, since it is a microseparation technique, unfolding studies can be applied to unpurified samples since it can resolve protein mixtures based on differences in  $\mu_{ep}$ . Biomolecular interactions involving receptor-ligand systems can also be examined, which can provide both thermodynamic and kinetic information. In most cases, unfolding results in a net decrease in  $\mu_{ep}$  due to increases in the frictional resistance of a denatured protein during electromigration. Thus, CE can be used as a probe to detect global changes in protein conformation. In addition, the specific type of detector in CE can also provide additional spectroscopic information, such as laser-induced native fluorescence (LINF) and electrospray ionization mass spectrometry (ESI-

MS). To date, most CE studies have examined protein unfolding via changes in temperature, pH and urea as a denaturant in the run buffer. One major constraint in CE is that Joule heating, which can result in non-specific changes in protein mobility, must be avoided when using conductive additives (e.g., guanidium chloride). Partial unfolding studies have also been performed with detergents (e.g. SDS)<sup>33</sup> and helical inducing agents (e.g., methanol)<sup>34</sup> to study intermediate conformations of protein unfolding. To date, few reports have applied CE to characterize protein unfolding involving receptors to small ligands, such as cAMP-dependent protein kinases. In this case, receptor-ligand binding results in a significant enhancement in protein conformational stability relative to the ligand-free receptor.

Protein unfolding studies in CE have typically been performed using on-capillary UV absorbance detection at 200 or 214 nm due to significant absorbance by aromatic amino acids residues and peptide bonds. Righetti reported differences in apparent thermodynamic parameters by measuring protein unfolding processes by CE at 214 and 280 nm, presumably due to the differential response of aromatic amino acid residues.<sup>31</sup> To date, there has only been a few reports of using CE with laser-induced native fluorescence (CE-LINF) for proteins with intrinsic tryptophan residues, which offers benefit of lower detection limits relative to UV absorbance



without the need for fluorescent labeling.<sup>35,36</sup> CE-ESI-MS represents a powerful hyphenated technique that has not been examined as a detector format to study protein unfolding to date. One major constraint for CE-ESI-MS is the need to use volatile buffers with low concentrations of salts or denaturants to minimize the extent of ion suppression, which can result in poor ionization efficiency. However, it has been demonstrated to be a promising technique for confirming partially denatured intermediates with modifications,<sup>37</sup> protein mixtures<sup>38</sup> and disulfide bond cleavages.<sup>39</sup>

### 5.2.3 Classical models of protein unfolding

Classic models for describing protein denaturation generally consider three major processes to be essential for understanding unfolding dynamics; namely the rate of unfolding, its reversibility (i.e., refolding) and the number of conformational states or intermediates that exist. Most protein unfolding studies in CE assume an ideal two-state system, where a protein denatures from an ordered, compact structure to an unfolded polypeptide, often considered as a random coil. In this case, protein unfolding occurs reversibly with negligible intermediate states being populated. Thus, the two major populations are the folded native (F) and unfolded (U) states (**equation 1.18**):



where  $k_1$  is the unfolding rate constant and  $k_2$  is the folding rate constant.

The populations of these states relate to the unfolding constant ( $K_U$ ):

$$K_U = \frac{[U]}{[F]} = \frac{k_1}{k_2} = \frac{f_U}{f_F} \quad (1.19)$$

As shown in **equation 1.19**,  $K_U$  is often expressed in terms of the ratio of fraction ( $f$ ) of the unfolded to folded protein as described below:

$$f_F = \frac{f_F}{f_F + f_U} = \frac{1}{1 + K_U} \quad (1.20)$$

$$f_U = \frac{f_U}{f_F + f_U} = \frac{K_U}{1 + K_U} \quad (1.21)$$

An increase in hydrodynamic radius is often associated with protein unfolding, which results in an apparent decrease in  $\mu_{ep}$ , assuming negligible changes in the net charge state of the protein. Protein unfolding plots in CE typically consist of measured viscosity-corrected protein mobility as a function of denaturant concentration or temperature. This generates a sigmoidal curve with a linear transition region from high to low mobility for the folded and unfolded protein states, respectively. Assuming a two-state system undergoing rapid unfolding with interconversion, the apparent viscosity corrected mobility of the protein ( $v\mu_{ep}^A$ ) within the

transition region is a weighted average of the mobilities of each fraction based on the following expression:

$$v\mu_{ep}^A = f_F\mu_{ep,F} + f_U\mu_{ep,U} = \frac{1}{1+K_U}\mu_{ep,F} + \frac{K_U}{1+K_U}\mu_{ep,U} \quad (1.22)$$

where  $\mu_{ep,F}$  is the mobility of the folded native protein and  $\mu_{ep,U}$  is the mobility of the unfolded protein. Note that for proteins unfolding under the slow-time regime in CE, direct measurement of the peak area ratio of the resolved folded and unfolded protein states are used to determine  $K_U$  in **equation 1.19** instead of  $v\mu_{ep}^A$  in **equation 1.22** or **equation 1.23**, which will be addressed in the next section.

#### 5.2.4 Urea Protein Unfolding Dynamics

Proteins can be chemically unfolded by the addition of chaotropic agents to the separation buffer such as urea,<sup>40</sup> which is compatible with CE studies since it is a neutral and UV transparent additive that does not contribute to Joule heating. However, the addition of high concentrations of urea (e.g., 7 M urea) required for complete protein unfolding can result in significant increases in solution viscosity, which needs correction to measure specific changes in protein mobility associated with unfolding. Within the transition region,  $K_U$  can be determined via the linear extrapolation method,<sup>41</sup> which was originally introduced for equilibrium

analysis by optical rotation methods. The equations have since been modified to be applied to other free solution studies, including CE, by rearrangement of **equation 1.22**:

$$K_U = \frac{v\mu_{ep}^A - \mu_{ep,F}}{\mu_{ep,U} - v\mu_{ep}^A} \quad (1.23)$$

where,  $K_U$  is the apparent protein unfolding equilibrium constant, which can be used to calculate the apparent free energy change for protein unfolding ( $\Delta G_U$ ):

$$\Delta G_U = -RT \ln K_U \quad (1.24)$$

$$\Delta G_U = \Delta G_U^0 - mc \quad (1.25)$$

Where,  $\Delta G_U^0$  is the standard free energy change for protein unfolding extrapolated to non-denaturing conditions (*i.e.*, 0 M urea),  $m$  is the cooperativity of unfolding which is related to the rate of change of  $G$  and  $c$  is the concentration of urea. The transition region is characterized by a mid-point concentration where there is an equal fraction of unfolded and folded protein states referred to as  $C_m$ . In general, a high  $C_m$  infers a conformationally stable protein more resistant to urea denaturation. Non-linear regression methods<sup>42</sup> can also be used to determine these parameters from the CE unfolding curve based on re-arrangement of **Equation 1.23-1.25**:

$$v\mu_{ep}^A = \frac{\mu_{ep,F} + \mu_{ep,U} \cdot e^{\frac{-(\Delta G_U - mc)}{RT}}}{1 + e^{\frac{-(\Delta G_U - mc)}{RT}}} \quad (1.26)$$

In folded protein states, most of the aromatic residues are buried in the hydrophobic core of the molecule, and upon unfolding they become exposed to the aqueous solvent. As the intrinsic tryptophan (Trp) fluorescence is a function of the polarity of the microenvironment, proteins that contain Trp results in changes in peak emission wavelength and fluorescence intensities are observed.<sup>43</sup> Thus, changes in mobility and fluorescence intensity can be used to assess protein unfolding dynamics when using CE with LINF detection.

### 5.2.5 Protein Unfolding Time Regime

Hilser and Freire<sup>44</sup> have defined unfolding time regimes as slow, intermediate and fast, relative to the timescale of CE separations. As depicted in **Figure 1.7 (a)**, in the slow time regime, the time required for electrophoretic separation is less than the time required for unfolding transitions ( $t \ll k_1^{-1} + k_2^{-1}$ ). Thus more than one peak is observed for each population state since they can be separated in time by CE based on differences in their  $\mu_{ep}$ . In this case, the protein does not interconvert during separation, and consequently, samples must be equilibrated or

incubated off-line prior to CE analyses. Also, unlike with fast time regime unfolding, a two-state assumption is not required, since unfolding intermediates can be resolved by CE. This is a unique advantage of CE based protein unfolding studies, since unlike conventional spectroscopic techniques, it allows for the direct measurement and resolution of protein intermediate conformers. In the fast time regime, the rate for protein folding or unfolding is much faster than the time required for separation ( $t \gg k_1^{-1} + k_2^{-1}$ ), which allows the different protein fractions to reach equilibrium. This situation results in the appearance of a single protein peak in the electropherogram as in **Figure 1.7 (c)**, which represents a weighted average of all populated states of the protein (e.g., two-state system). Since equilibrium is reached well before the sample zone migrates past the detector, unfolding studies by CE can be performed dynamically in-capillary without off-line pre-equilibration. This allows for rapid analysis time and reduced consumption of protein since the same sample (< 50  $\mu\text{L}$ ) can be re-injected throughout the entire study. Hilser and Freire<sup>44</sup> also describe an intermediate time regime, as illustrated in **Figure 1.7 (b)**. In this time regime, the length of time required for electrophoretic separation is long enough to allow only a fraction of the protein conformations to interconvert between the folded and unfolded states, while others remain unchanged ( $t \sim k_1^{-1} + k_2^{-1}$ ). This results in the

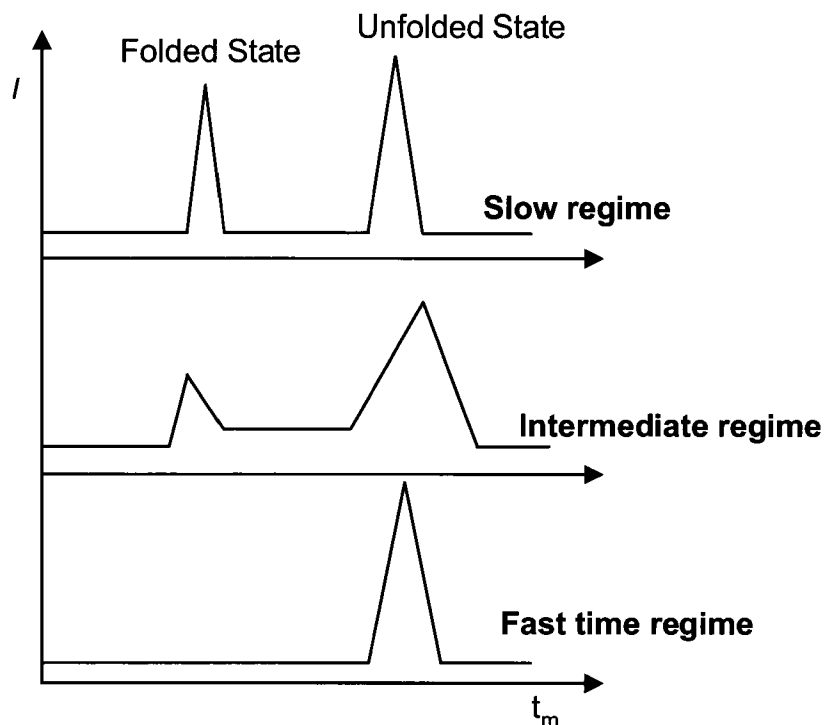


**Figure 5.3** Simulated unfolding time regimes for proteins undergoing reversible two-step denaturation by CE in the (a) slow ( $t \ll k_1^{-1} + k_2^{-1}$ ), (b) intermediate ( $t \sim k_1^{-1} + k_2^{-1}$ ) and (c) fast time regime ( $t \gg k_1^{-1} + k_2^{-1}$ ).

appearance of a raised band between the peaks representing partial folded/unfolded conformations and is a common indicator of a multi-step process, where intermediate conformations cannot be assumed to be negligible. In fact, some previously described two-state proteins such as ribonuclease S6 are demonstrated to have unfolding intermediates.<sup>45</sup> CE conditions can be optimized (e.g., capillary length, applied voltage, preincubation time) to improve protein peak resolution in cases where

intermediate time regime unfolding processes are initially observed. Thus, an understanding of the kinetics of protein unfolding is an important feature when performing CE experiments that permit either direct dynamic in-capillary unfolding or equilibration unfolding studies after pre-incubation.



### 5.3 References

---

- 1 Bosch L.I., Fyles T.M., James T.D., *Tetrahedron* **60** (2004) 11175-11190.
- 2 Draffin S.P., Duggan P.J., Duggan S.A.M., *Org. Lett.* **3** (2001) 917-920.
- 3 Liu X., Hubbard J., Scouten W., *J. Organomet. Chem.* **493** (1995) 91-94.
- 4 Yang W., Gao S., Gao X., Karnati V.R., Ni W., Wang B., Hooks W.B., Carson J., Weston B., *Bioorg. Med. Chem. Lett.* **12** (2002) 2175-2177.
- 5 Yan J., Springsteen G., Deeter S., Wang B., *Tetrahedron* **60** (2004) 11205-11209.
- 6 Springsteen G., Wang B., *Tetrahedron* **58** (2002) 5291-5300.
- 7 Lorand J.P., Edwards J.O., *J. Org. Chem.* **24** (1959) 769-774.
- 8 Davis A. P., Wareham R. S., *Angew. Chem., Int. Ed.* **38** (1999) 2978-2996.
- 9 James, T. D. In Boronic Acids Preparation, *Applications in Organic Synthesis and Medicine: Boronic Acid-based Receptors and Sensors for Saccharides*; Hall, D., Ed.; Wiley-VCH: Weinheim, (2005).
- 10 Wright A.T., Anslyn E.V., *Chem. Soc. Rev.* **35** (2006) 14-28.
- 11 Zaubitzer F., Buryak A., Severin K., *Chemistry-Eur. J.* **12** (2006) 3928-3934.
- 12 Lee J. W., Lee J.S., Chang Y.T., *Angew. Chem.* **118** (2006) 6635-6637.
- 13 Schiller A.; Wessling R. A.; Singaram C., *Angew. Chem., Int. Ed.* **46** (2007) 1-4.
- 14 Wamelink M., *J. Inher. Metab. Dis.* **28** (2005) 951-963.
- 15 Lee J., *J Chromat B* **831** (2006) 126-131.
- 16 Brogard J.M., Caro-Sampara F., Blicke J.F., *La Revue de médecine interne* **13** (1992) 69-79.
- 17 Schmidt, R., *J. Neuropathol. Exp. Neurol.* **57** (1998) 1175-1189.
- 18 Vinet B., *Clin. Chem.* **44** (1998) 2369-2371.
- 19 Barboza M. *J. Med. Biol. Res.* **32** (1999) 1499-1504.
- 20 Shinka T., *J. Chrom. B.* **732** (1999) 469-477.
- 21 Heller W., Vigil D., Brown S., Blumenthal D., Taylor S.S., Trehwella J., *J. Biol. Chem.* **279** (2004) 19084-19090.

- 
- 22 McCoy M. et al. *JACS Communications* **127** (2005) 7978-7979.
- 23 Shabb, J. B., *Chem. Rev.* **101** (2001) 2381-2411.
- 24 Amieux P. et al, *Annals of the New York Academy of Sciences* **968** (2002) 75-95.
- 25 Cummings D. et al., *Nature* **382** (1996) 622-626.
- 26 Gullingsrud J., *Structure* **14** (2006) 141-149.
- 27 Makhatadze, G.I. *In Protein Folding Handbook*. Buchner J., Kiefhaber T., Ed., Wiley-VCH, **1** (2005) 70-98.
- 28 Bruylants G., Wouters J., Michaux C., *Curr. Med. Chem.* **12** (2005) 2011-2020.
- 29 Gavina J.M.A., Britz-McKibbin P., *Curr. Anal. Chem.* **3** (2007) 17-31.
- 30 Rush R.S., Cohen A.S., Karger B.L., *Anal. Chem.* **63** (1991) 1346-1350.
- 31 Righetti P.G., Verzola B., *Electrophoresis* **22** (2001) 2359-2374.
- 32 Rochu, D., Ducret, G., Ribes, F., Vanin, S., Masson, P., *Electrophoresis* **20** (1999) 1586-1594.
- 33 De Lorenzi E., Grossi S., Massolini G., Giorgetti S., Mangione P., Andreola A., Chiti F., Bellotti V., Caccialanza G., *Electrophoresis* **23** (2002) 918-925.
- 34 Verzola B., Perduca M., Mezo G., Hudecz F., Righetti P.G., *Electrophoresis* **24** (2003) 794-800.
- 35 Fan Z.H., Jensen P.K., Lee C.S., King J., *J. Chromatogr. A* **769** (1997) 315-323.
- 36 Jensen P.K., Lee C.S., King J.A., *Anal. Chem.* **70** (1998) 730-736.
- 37 Heegaard N.H.H., Rovatti L., Nissen M.H., Hamdan M., *J. Chromatogr. A* **1004** (2003) 51-59.
- 38 Stutz H., Bordin G., Rodriguez A.R., *Electrophoresis* **25** (2004) 1071-1089
- 39 Thannhauser T.W., Rothwarf D.M., Scheraga H.A., *Biochemistry* **36** (1997) 2154-2165.
- 40 Kilar F., Hjerten S., *J. Chromatogr. A* **638** (1993) 269-276.
- 41 Greene R.F., Pace C.N., *J. Biol. Chem.* **249** (1974) 5388-5393.

- 
- 42 Verzola B., Chiti F., Manao G., Righetti P.G., *Anal. Biochem.* **282** (2000) 239-244.
- 43 Sharma V. J., *Pharmac. Sc.* **92** (2003) 890-899.
- 44 Hilser V.J., Freire E., *Anal. Biochem.* **224** (1995) 465-485.
- 45 Otzen D., *Protein Eng. Des. Sel.* **18** (2005) 547-557.